Open Medscience

Peer-Reviewed Open Access

JOURNAL OF DIAGNOSTIC IMAGING IN THERAPY

Journal homepage: www.openmedscience.com

Review Article

A review of 3D image-based dosimetry, technical considerations and emerging perspectives in ^{90}Y microsphere therapy

Jim O' Doherty*

PET Imaging Centre, Division of Imaging Sciences and Biomedical Engineering, King's College London, King's Health Partners, St. Thomas' Hospital, London, United Kingdom

*Corresponding author:
Jim O' Doherty, Ph.D.
Email: jim.odoherty@kcl.ac.uk

Abstract

Yttrium-90 radioembolization (^{90}Y-RE) is a well-established therapy for the treatment of hepatocellular carcinoma (HCC) and also of metastatic liver deposits from other malignancies. Nuclear Medicine and Cath Lab diagnostic imaging takes a pivotal role in the success of the treatment, and in order to fully exploit the efficacy of the technique and provide reliable quantitative dosimetry that are related to clinical endpoints in the era of personalized medicine, technical challenges in imaging need to be overcome. In this paper, the extensive literature on current ^{90}Y-RE techniques and challenges facing it in terms of quantification and dosimetry are reviewed, with a focus on the current generation of 3D dosimetry techniques. Finally, new emerging techniques are reviewed which seek to overcome these challenges, such as high-resolution imaging, novel surgical procedures and the use of other radiopharmaceuticals for therapy and pre-therapeutic planning.

ISSN: 2057-3782 (Online)
http://dx.doi.org/10.17229/jdit.2015-0428-016

Keywords: dosimetry; molecular radiotherapy; ^{90}Y microspheres; Monte Carlo; hepatocellular carcinoma

1. Introduction

The primary form of liver cancer (hepatocellular carcinoma - HCC) is the second largest contributor to cancer mortality in the world, and is the second most common cause of death from cancer worldwide, estimated to be responsible for 746,000 deaths in 2012 (9.1% of the total) [1]. In Europe, 63,500 new cases of liver cancer were diagnosed in 2012 [2]. The prognosis for HCC is poor, with 5-year survival rates (dependent on staging) in England approximately 5.5% [2] and in the United States less than 15% [3].

The liver is also a common metastatic site for tumours in organs drained by the portal vein such as from colorectal, pancreatic and stomach malignancies [4]. HCC and liver metastases represent different tumour types, with more peripheral vascularization in HCC and a higher proportion of smaller lesions in metastases [5]. Similar to primary HCC, surgical resection of metastases is usually considered the best curative practice, although only approximately 25% of patients are eligible [6].

The liver possesses unique vascular anatomy due to its dual blood supply. Normal hepatic tissue obtains over 70% of its blood supply from the portal vein while intrahepatic malignancies derive their blood supply almost exclusively via the hepatic artery [7]. Using this process, intra-arterial techniques such as radioembolisation of radioactive microspheres (RE) can selectively target the liver malignancies. RE typically employs 90-yttrium microspheres (^{90}Y-MS - β-emitter, $t_{½}$ =64.2 hours, $E_{β(av)}$=0.94 MeV, average tissue penetration = 2.5 mm max. range = 1.1 cm) of which there are currently two types commercially available; a glass microsphere (TheraSphere, BTG Inc./MDS Nordion Inc., Ottawa, Canada) and a resin microsphere (SIRTeX Medical Ltd, Sydney, Australia) hereon denoted GMS and RMS respectively. The properties of these MS are detailed in Table 1. Since approval of these devices, a rapid increase in the amount of publications indicating their use has been published (see Figure 1).

Evidence has been mounting regarding the ability of a measurement of the absorbed dose to tumour to help predict the tumour response and patient outcome, although dosimetry rarely finds routine clinical use despite response being a key parameter in the clinic [8]. A recent review by the EANM Dosimetry Committee identified 48 papers (out of 79 surveyed) employing the use of radionuclide dosimetry showing a strong correlation between absorbed dose and the tumour response & toxicity over a wide range of radionuclide treatments (including ^{90}Y-RE) [9], and many works have noted the lack of randomized trials comparing dosimetry-based radionuclide therapy to fixed dosing, or dosing per kg body weight [10, 11]. For routine use, there is a requirement of standardized procedures for absorbed dose calculations [12] and improved reliability of radiobiological models used to convert dosimetric data to biologic endpoints [13].

^{90}Y-RE treatment planning should be based on *a priori* knowledge of the radiobiological effects to predict the total absorbed tumour/normal liver doses (hereon denoted D_T and D_{NL} respectively) and intended responses before or during the therapeutic intervention, as is common in brachytherapy or external beam radiotherapy (EBRT). The principle disadvantages of patient-specific dosimetry for ^{90}Y-RE centre around logistical aspects and enabling of resources/time [14].

	SIR-Spheres	**TheraSphere**
Radioisotope	^{90}Y	
Isotope location	Attached to surface	Incorporated into glass matrix
β emission (MeV)	2.28 (100%)	
ϒ emission	None	
Matrix material	Resin	Glass
Density (g/mL)	1.6 [15]	3.2 [15]
Av Diameter (μm)	32±10 [15]	25±10 [15]
Number of particles (range)	30-60 x10^6 [16]	3-8 x 10^6 [16]
Bq per sphere	50 [16]	2500 [16]
Embolic effect	Mild-moderate	Mild
Available activity (GBq)	3	3, 5, 7, 10, 15, 20
Shelf life	24 hours	12 days
Endpoint	Target Activity/stasis	Target Dose

Table 1. Parameters of RMS and GMS for ^{90}Y-RE.

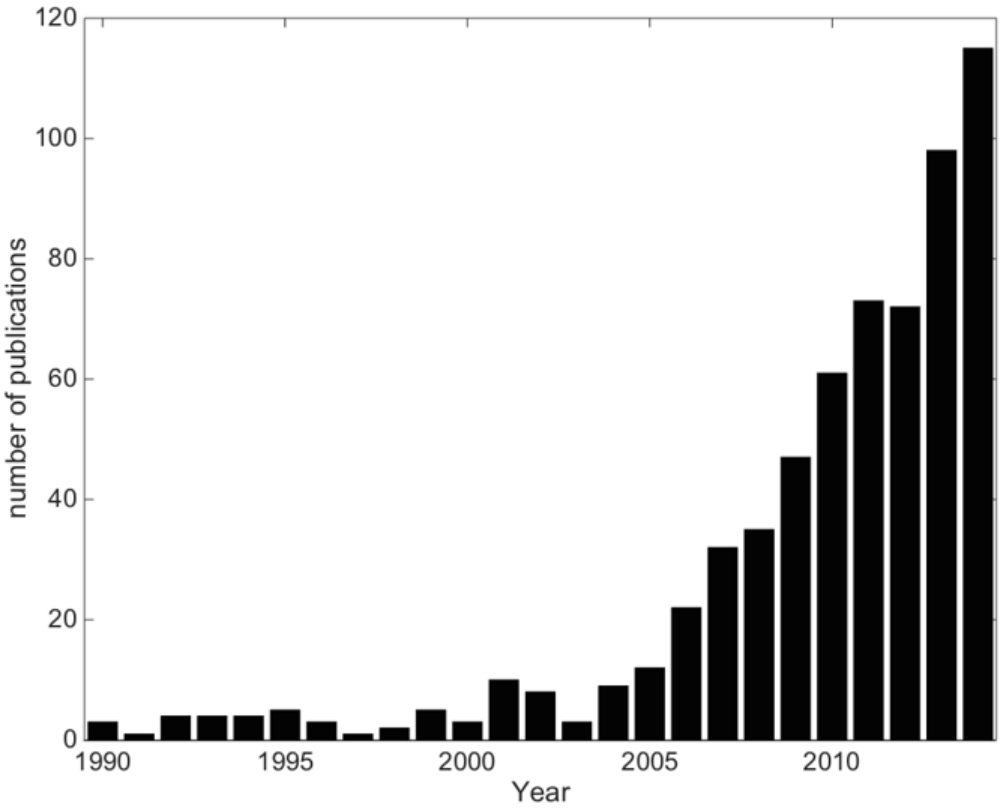

Figure 1. The growth in publications related to ^{90}Y-RE as of Jan. 1st 2015. An online publication search http://www.ncbi.nlm.nih.gov/pubmed/ had the following search conditions: text strings "Microspheres" or "radioembolization" to appear in Title/Abstract and "90" to appear in the Title/Abstract. The final publication list was manually filtered for relevant publications and sorted by date.

http://dx.doi.org/10.17229/jdit.2015-0428-016

Quantitative data acquisition procedures are complex and demanding and require significant expertise to ensure the integrity of data, reduction of errors and reliability of the methodology. It is with this in mind that current techniques of ^{90}Y-RE are reviewed such as factors affecting accurate quantification, 3D-dosimetry techniques, and emerging techniques that may further help the efficacy of the technique in providing reliable predictive clinical endpoints.

2. Current Techniques

2.1 Procedure

Implantation of ^{90}Y-MS is typically a 2-stage process, a 'mapping' phase and later (usually 1-2 weeks) an implantation phase. The mapping step is carried out using a microcatheter guided via fluoroscopy through the common hepatic artery. Extrahepatic branches to critical organs are identified and prophylactically embolized in order to limit the potential deposition of MS to the critical organs. Although outside the scope of this review, the reader is referred to excellent reviews related to the angiographic mapping procedure [17].

Once the mapping and embolization steps are complete, ^{99m}Tc-MAA (75 MBq - 150 MBq, hereafter denoted 'MAA') is injected through the catheter where the albumin particles are trapped in the first arteriolar–capillary bed encountered. The properties of MAA are summarized in Table 2. The patient is then taken to a gamma camera and a scan performed for the purpose of confirming access to the liver by the delivery system, excluding access to extra-hepatic sites, and defining the extent of shunting to the lungs (described below).

Parameter	MAA
Radioisotope	^{99m}Tc
Isotope location	Attached to surface
β emission	None
ϒ emission	141 keV (89%)
Matrix material	Aggregated human serum albumin
Density (g/mL)	1.1
Av Diameter (μm)	10-60
Number of particles (range)	0.15 x 10^6
Bq per sphere	-
Embolic effect	Mild
Available activity (GBq)	Any
Shelf life	Dissociation after 2 hours
Endpoint	Target Activity

Table 2. Typical parameters of ^{99m}Tc-MAA for pretherapy assessment.

Concerning pretherapy imaging, there is broad agreement on SPECT-CT being more clinically useful in terms of extrahepatic uptake and more accurate in terms of activity quantification than either SPECT or planar imaging [18,19,20] with a recent study of 58 patient scans showing rates of detection of extrahepatic MAA was 72%, 79% and 96% for planar, SPECT and SPECT-CT, respectively [21]. Other

studies have identified extrahepatic uptake on SPECT-CT not discernible on planar or SPECT only, leading to treatment adjustments such as additional surgical embolization [18,22]. Other work shows a sensitivity of 100% of using SPECT-CT to detect extrahepatic uptake compared to 41% for non-attenuation corrected SPECT and 32% for planar imaging respectively [22]. Recently also evaluated is the discordance between hepatic angiography and MAA SPECT, noting severe discordance in only 3 of 74 cases of patients with HCC [23].

The ^{90}Y-MS implantation involves repeating the catheterization procedure on the treatment day. Extra mapping may be performed to examine the viability of previously implanted embolization coils, and further coil embolizations may be attempted as the time difference between the MAA and MS treatment may allow for the development of arteriovenous anastamoses. ^{90}Y-MS are then infused through the hepatic arteries under fluoroscopic guidance, with caution paid to any reflux of spheres. The activity of MS to be implanted is dependent on factors such as the type of spheres used, properties of the target site (i.e. primary HCC or metastatic tumours) and the level of lung shunt determined from the MAA scan, Typically, after the procedure is complete, the patient is again taken to a gamma camera and Bremsstrahlung imaging performed to localize the MS.

2.2 Activity Planning

2.2.1 Resin Microspheres (RMS)

An empirical method was devised based on the intraoperative calculations from beta probes of early clinical trials [24], providing tables of activity-dependent only on liver tumour volume. Tumour involvement that was < 25%, 25%–50%, or > 50% of the total liver volume was treated with 2 GBq, 2.5 GBq, or 3 GBq respectively. A U.S. Consensus panel some years ago recommended discontinuation of this method [25], as the high risk of REILD in small livers of early clinical trials using this method was confirmed in a multicenter study [26].

In the body surface area (BAS) method, the administered activity is calculated as a function of the liver tumour volume and the patient size by the empirical equation:

$$\boldsymbol{A\,[GBq] = (BSA\,[m^2] - 0.2) + \left(\frac{V_{tumor}}{V_{liver}}\right)} \qquad (1)$$

where BSA (m^2) is calculated as 0.20247 × height (m)$^{0.725}$ × weight (kg)$^{0.425}$. V_{tumour} and V_{liver} represent the volumes of tumour and total liver respectively. A multiplicative factor is recommended concerning whole lobar treatments:

$$\boldsymbol{A[GBq] = \left(BSA\,[m^2] - 0.2 + \frac{V_{tumor}}{V_{lobe}}\right) \times \frac{V_{lobe}}{V_{liver}}} \qquad (2)$$

ISSN: 2057-3782 (Online)
http://dx.doi.org/10.17229/jdit.2015-0428-016

This method is the most common because of its ease of implementation, requiring only measurements of the tumour volume and patient height and weight, and an online tool is available to aid the user in activity calculation http://apps01.sirtex.com/smac/.

Early clinical trials with RMS noted the presence of radiation pneumonitis (RP) post-treatment [27]. Modifications to injected activity were proposed depending on the level of hepatopulmonary shunting (LS) of MS through arteriovenous vessels bypassing the capillary bed to the lungs, as an absorbed dose of 30 Gy to lungs (D_{LUNG}) has been suggested to cause RP [28]. The manufacturer of SIR-Spheres and recent guidelines recommend less than 25 Gy and preferably less than 20 Gy [29,30]. The lung shunt fraction is calculated as LSF=lung counts/(liver counts + lung counts), and is a multiplicative modification to the ^{90}Y activity determined by Eqn 1 (LS<10% LSF=1; 10-15% LSF=0.8; 15-20% LSF=0.6; >20% no treatment).

Via MIRD calculations, the target organ dose is calculated as the product of the cumulated activity in the organ and the corresponding organ S-value [31], and the total target dose is the summation of all source organ contributions. However the use of organ level S-values inherently assuming uniform activity distribution in the organ, and the use of standardized anatomical models are the major limitations to the technique. Complete reviews of the principles of organ-level MIRD dosimetry relating to ^{90}Y-MS are available in the literature [32].

The partition model (PM) incorporates tissue masses and a measurement of the tumour-to-normal tissue (TN) ratio [33]. It requires separation of the organ system into compartments (normal liver, lungs and tumour), and setting prescribed safe radiation doses whereby the maximum administered activity does not exceed these dose limits (80 Gy to normal functioning liver [34], (70 Gy for patients with cirrhosis [34]) and less than 25 Gy to the lungs [27]). The activity required for implantation (A_{TOTAL}) is calculated based on a limiting lung dose, and also for a limiting D_{NL}:

$$\boldsymbol{A_{TOTAL}(lung) = \frac{D_{LUNG} \times M_{LUNG} \times LSF}{49670}} \quad (3)$$

$$\boldsymbol{A_{TOTAL}(normal\ liver) = \frac{D_{NL} \times (M_{LIVER} + TN \times M_{TUMOR})}{49670 \times (1 - LSF)}} \quad (4)$$

where M_{LIVER}, M_{LUNG}, and M_T represent the masses of normal liver, lungs and tumour (in g) respectively.

The *TN* ratio is the ratio of activity in the tumour (A_T) and normal liver (A_{NL}) per unit mass (M_T and M_{NL} respectively) of the compartment as determined from the MAA scan:

$$\boldsymbol{TN = \frac{A_T / M_T}{A_{NL} / M_{NL}}} \quad (5)$$

It should be noted that this is an *estimate* of the TN, and may not always be the same as the *true* TN.

http://dx.doi.org/10.17229/jdit.2015-0428-016

2.2.2 Glass Microspheres (GMS)

The activity for administration of GMS relates directly to the desired absorbed dose based on a nominal target dose (150 Gy/kg), and assumes a uniform distribution of microspheres throughout the liver. A general equation for determining the activity based on 2-compartmental MIRD macrodosimetry is written as:

$$A_{TOTAL}[GBq] = \frac{D_{TARGET}[Gy] \times M_{TARGET}[kg]}{49.7\ [Gy \cdot kg/GBq]} \quad (6)$$

where M_{TARGET} is the mass of the target (i.e. whole liver or liver lobe, or lungs). There are no adjustments to the ^{90}Y activity based on LSF; the treatment proceeds provided D_{LUNG} <30 Gy (single treatment) and <50 Gy (cumulative treatment). The maximum activity is calculated based on a limiting dose of 30 Gy to the lungs taking into account the LSF:

$$A_{MAX} = \frac{30 \times M_{LUNG}}{LSF \times 49.7} \quad (7)$$

From Eqn 6, the liver dose can be defined as:

$$D_{total\ liver} = \frac{49.7 \times A_{TOTAL}(1-LSF) \times (1-R)}{M_{total\ liver}} \quad (8)$$

where *R* represents the percentage of the total activity remaining in the vial after treatment. Thus, the absorbed dose is highly dependent on how the liver mass is calculated.

2.3 Differences between RMS and GMS

There are clear differences between GMS and RMS, and there is an ongoing debate as to whether these differences lead to different efficacy and toxicity profiles [35,36]. Although it has been postulated that the optimal combination of specific activity and embolic load is somewhere between that of GMS and RMS [37], recent work shows that the overall survival of patients treated with either GMS or RMS across different HCC stages is quite consistent [38]. A multicentre study of hepatic metastatic neuroendocrine tumours showed a statistically significant greater median absorbed dose to liver lobes delivered using GMS (right 117 Gy, left 108 Gy) than using RMS (right 50.8 Gy, left 44.5 Gy), although a similar disease control rate for both (92% GMS and 94% RMS were partial responders or stable disease) after 6 months [39]. More fundamentally, computer simulations have demonstrated the absorbed dose deposited around a point source of resin and glass spheres shows differences of 1% to be with 1% of each other [40].

Recent studies have shown a relatively large difference in microscopic radiobiology between GMS and RMS behaviour, and that the lower number of GMS used for treatment provides a less uniform

irradiation, thus allowing a mean whole liver absorbed dose (D_{WL}) of 120 Gy with no toxicity to the radiosensitive portal triads [41,42], or 150 Gy for single treatment (268 Gy for repeat administrations) [43]. Their results provide reasoning to the D_{NL} threshold noted in other clinical studies of 70 Gy using GMS [44] and approximately 40-50 Gy using RMS [13,45]. It should be noted that although no toxicity was noted with absorbed doses of up to 100 Gy [46], the manufacturer of RMS recommends a D_{NL} of 80 Gy and a recent summary suggests a preferable D_{NL} of 50 Gy [29]. Toxicity of either GMS or RMS is not only dependent on the dose volume factors, but also on the patient population, underlying liver disease, liver function and concurrent therapies [47].

Stasis represents the main reason for stopping the delivery of RMS before full planned activity is given due to the high number of spheres (20 million/GBq), and is not desired in part because of shunting into normal liver causing tumour hypoxia [26]. Due to the lower number of GMS typically encountered (400,000/GBq), stasis and embolic effects have yet to be reported [28]. Therefore because of the mechanics of sphere deposition, a higher injected activity may not always lead to a higher D_T. In a recent editorial, it was noted that the specific activity and number of spheres per GBq should be considered a crucial variable and thus reported in clinical trials [48].

3. Current issues in ^{90}Y therapy

3.1 Assaying the Activity

Error in assaying the activity against the manufacturer determined activity creates further errors in absorbed dose calculations. Although this verification is a fundamental requirement on which all quantitative measurements are made, measurement of vial activity of ^{90}Y-MS remains an important issue due to lack of standardization in measurements [49,50]. Due to Bremsstrahlung production, the activity measurements made in a dose calibrator vary with sample geometry, vial placement within the calibrator, vial thickness and solution volume. RMS activity can also vary widely when in a settled state compared to suspended state (distributed homogenously) in the vial. For example, a 20% difference was noted in MS activity dependent on the material of the V-vial compared to shipping vial [50]. One study noticed a 2-16% variance of the MS activity when compared to a reference source between 5 sites participating in a multicentre study employing RMS [26]. Owing to these factors, a total dose delivery error on the order of 20% is noted as possible [49].

There are also no current traceable standards in the UK, or USA for RMS, although there is a NIST traceable calibration for GMS. Correction factors can be employed although this is not trivial process [51]. It is recommended to characterize the local activity measurement standard rather than accepting the calibration value of the calibrator manufacturer [50]. A previous work investigated a spectroscopic assay of the ^{90}Y positron decay of resin spheres measuring an activity 26% higher than manufacturer indicated [52].

A dedicated work package of the ongoing European project MetroMRT (**METRO**logy for **M**olecular **R**adio**T**herapy) is aiming to provide traceable dosimetry standards for ^{90}Y-RE procedures, and is described further below.

3.2 Limitations of current dosimetry models

Recent work has noted that there is no known association correlating a patient's BSA with liver volume, tumour volume or radiation sensitivity [53]. Inherent in the BSA method is the assumption of a fixed mean TN liver ratio of 1 for all patients, sacrificing accuracy for simplicity, although patients typically present with a more favourable ratio [19]. A recent retrospective study of 45 patients with liver metastases treated by RMS showed that using Eqn. 1, the administered activity does not correlate with D_{WL} [54], with a 2.5 fold difference in D_{WL} over all patients. They did, however, find a correlation between liver weight and D_{WL}, noting that patients with large livers are relatively under-dosed, and patients with smaller livers are overdosed using this technique.

A recent study compared activity planning and dosimetry in 26 patients with RMS using 4 models (BSA, empirical and PM) showing that maximum differences in injected activities between BSA and PM methods vary from 123%-417% [55]. Although it has been noted that the PM would be the preferred method of ^{90}Y-RE for every patient [55,56], its main drawbacks are the reliance on segmentation of tumour/non-tumour for activity determination and dosimetry purposes, and the assumption of concordance between the MAA (from which the TN ratio is calculated) and MS distribution. This assumed equivalency is a fact much disputed by recent studies, especially in liver metastases [57,58] and is described further below. In clinical scenarios, the PM and GMS equations are employed mainly in patients with hypervascular, large and numerically limited lesions, such as HCC.

In many metastatic cases, clear definition of the tumour boundaries proves difficult due to diffuse metastatic spread and differing vascularity [5], and therefore the PM proves difficult to apply. Recent work shows it cannot be recommended in general for patients with liver metastases [57,59]. This model also disregards the spatial and temporal variation of the dose, dose rate and radiobiological effects, providing a simplified picture for patient dosimetry [60].

3.3 Determination of lung shunt fraction (LSF)

Dissociation of ^{99m}Tc-MAA into free pertechnetate ($^{99m}TcO_4^-$) has been known to change the patient LSF classification and also degrade the image quality [61]. Clinical reporting issues also exist relating to dissociation; in a recent study, uptake in the stomach could not be attributed either to pertechnetate or true MAA uptake [61]. In certain clinics, patients undergoing RMS treatment are pre-treated with sodium perchlorate before angiography, which aids in preventing unspecific uptake of MAA in the stomach and thyroid [22,62].

A recent study has shown that increasing LSF results when scanning patients at later timepoints [62]. At <1 hour after MAA injection a LSF of 7.1% was calculated, whereas at >4 hours, an LSF of 21.6% was determined. The kinetics of MAA due to degradation over time have also largely been ignored [49]. Provided the technique is performed correctly, the LSF estimation is reproducible, even despite different catheter positions when repeated on the same patient [61].

The use of scatter correction routines during planar image acquisition for LSF determination in RMS treatments has been shown to have an effect on LSF, with a reduction of 50% of the lung shunting percentage, potentially moving patients into different LSF classifications [63]. There is a further reduction in LSF using SPECT whereby volumes of interest are used instead of planar regions. It has also recently been shown that without CT attenuation correction (AC), the LSF can be overestimated by up to 65% on average of 26 patients receiving RMS treatment, and without AC would have resulted in reduced MS activity for 7 patients and excluded 1 from treatment entirely [55].

3.4 Quantitative ^{90}Y reconstruction

Bremsstrahlung imaging suffers from poor resolution (approximately 10-15 mm), primarily due to the lack of a pronounced photopeak. The wide range (0 – 2.3 MeV) and continuous nature of the spectrum prohibit the use of energy window based scatter rejection/correction techniques. Other processes that confound corrections include AC (based on a single photon energy), collimator scatter, lead X-rays, septal penetration, camera backscatter and partial energy deposition in the crystal [64].

For gamma cameras, a common calibration method is to use a large phantom filled with ^{90}Y [65] or a vial of activity [66]. Images are then reconstructed, and a calibration factor derived from region measurements compared to the known activity concentration.

Recent efforts have shown an improvement in the quantitative accuracy of ^{90}Y imaging through the use of Monte Carlo (MC) based modelling of the image degrading factors. Simulations can be performed to calculate energy-dependent scatter kernels and collimator-detector response (CDR) tables which can be applied during image reconstruction [65]. This method showed that activity in a large source such as the liver was estimated with a bias of around −70%, when no compensations were included, whereas with compensations, bias was reduced to -10% to 16%. Similar work along with a model of the decay location and photon emission location incorporated into an OSEM reconstruction, showed increased quantitative accuracy validated on digital (XCAT) and physical phantoms with errors between -1.6% and 11.9% [67]. Other work provides real-time MC simulations of scatter and attenuation effects for each patient, and is less dependent on patient geometry [68].

They show improved image contrast and decreased count error compared to non-MC SPECT reconstruction, and also a more accurate mean absorbed dose to a phantom. A recent quantitative SPECT dosimetry guideline recommends the use of MC based corrections for Bremsstrahlung imaging [69] however the routine clinical implementation of such corrections is not easily applied.

In a comparison of collimators for ^{90}Y Bremsstrahlung imaging, recent phantom work showed that a medium energy pinhole (MEPH) collimator (or multi-pinholes) and the inclusion of a scatter model provided similar results to TOF (time of flight) PET in terms of contrast recovery and image quality [70].

3.5 Using ^{99m}Tc-MAA as a ^{90}Y MS surrogate

Using ^{99m}Tc-MAA biodistribution as a dosimetry predictor for MS implantation is an attractive option whereby the MAA scan can be used to determine the desired activity of ^{90}Y-MS to be injected to achieve a prescribed D_T. However, different physical properties, surgical procedures and timing between catheterizations result in MAA being an imperfect surrogate for GMS and RMS [23,71,72]. Recent discussions observe that discordance in MAA-microsphere distribution may be attributable to the differing vascularity of HCC and metastases [59], with a suggestion of a more concordant relationship in HCC cases [73].

In terms of size, arterioles feeding liver metastases have a diameter of 30-40 μm, and thus larger MAA particles are likely to embolize outside the metastatic tissue [72]. Thus, existing differences in flow between metastatic lesions of variable size are likely to be exaggerated on MAA imaging when compared to MS imaging. In recent work, the visual correlation between co-registered MAA distribution and RMS distribution for 20 patients with hepatic metastases ranged from high to very poor, with a mean Spearman rank correlation of 0.65 [74]. A study of RMS in 39 patients (with both HCC & metastatic lesions) segmented the liver into segments, and showed that for 68% of all segments (n=225), a difference of >10% between MAA and MS activity distribution was found, and that in every procedure at least 1 segment showed a >10% difference [58]. A similar study of 81 patients with a mix of HCC and metastases treated with RMS showed 31 patients had segmental perfusion differences, influenced highly by catheter position [75]. A recent study of 18 HCC patients treated with RMS found that the ratio of MAA to MS uptake in the tumour was 1.4:1, indicating that using MAA imaging for dosimetry calculations can overestimate D_T [76].

Surgical procedures have been identified as a cause of MAA-MS mismatch such as differences in injection rates, microcatheter positioning [75] and arterial flow hemodynamics [23]. A 5-10 mm difference in catheter position between tip and artery opening has been shown to have a major impact on microsphere flow distribution [58,77]. Fluid dynamic models of MS transport in a hepatic arterial system highlight the influence of the injection time interval, specific daughter vessel targeting, microsphere injection velocity, and vessel morphology [78,79].

3.6 Microsphere distribution

Fundamentally, MS methodologies are based on the assumption of uniform distribution within tumour/non-tumour compartments. Early investigations into RMS localization examined ex-vivo liver tissue samples to measure the distribution of RMS showing clustering of microspheres around the

tumour periphery [80]. Approximating a liver neoplasm as a sphere, 90% of all microspheres were found in a 6 mm periphery zone around an inner avascular core (there were 50-70 times more spheres in the periphery zone than in the normal liver). Further work assuming each sphere as a point source of radiation, showed a large difference in average D_{NL} compared to the MIRD method (8.9 Gy vs. 80 Gy) [81].

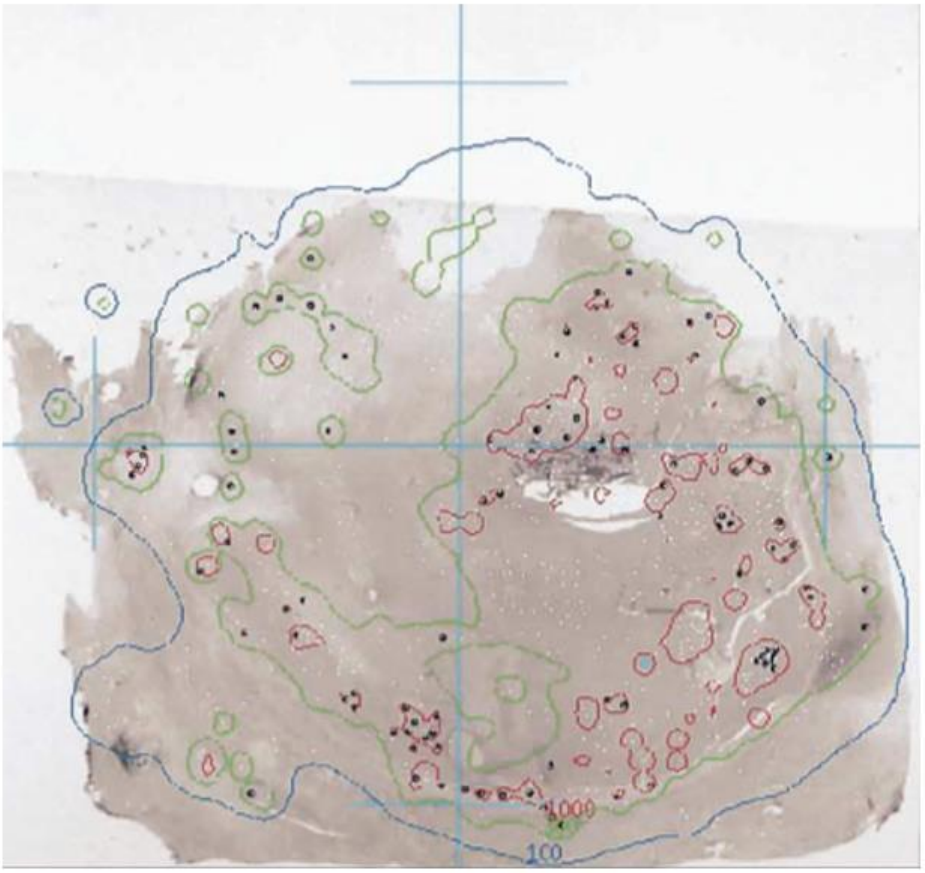

Figure 2. Photomicrograph showing a mid-plane tissue sample with RMS (black dots). White dots represent sphere positions from sections anterior and posterior to the slice shown. Overlaid are the 100 Gy (blue) and the 1000 Gy (red) isodose curves. Reproduced with permission [15].

Using a MC dose deposition technique, the heterogeneous nature of dose distribution with ranges of 25 Gy to 3,000 Gy over a 4 cm area for 4 explanted livers was shown [15]. An example of this high dose range is shown in Figure 2. This work showed similar clustering for GMS, noting high doses to tumour/normal tissue boundary, and not observing any difference in the embolic location of GMS or RMS.

More recent work with RMS in liver biopsies showed on average 8 to 59 spheres per cluster, with an activity concentration of 1040 and 3050 Bq/mg for 2 patients [82]. Similar levels of clustering were also shown in simulations of GMS in different arterial tree models when the difference in number of spheres is taken into account [41].

4. Dosimetry Methods in ^{90}Y-RE

4.1 Direct Monte Carlo

By the introduction of a complete anatomical dataset (usually a CT scan) and a quantitative map of cumulated activity (PET or SPECT images) into a generalised model of radiation transport, an accurate means of calculating patient-specific absorbed dose distributions can be obtained through the use of MC simulations. The technique allows the assessment of heterogenous dose distribution in targets via the use of dose volume histograms (DVH).

Direct MC methods are based on general-purpose radiation transport codes of which there are many: EGS or EGSnrc (electron gamma shower), MCNP (Monte Carlo N-Particle), PENELOPE (PENetration & Energy Loss of Positrons and Electrons) and FLUKA (FLUktuierende KAskade). A toolkit more tailored to nuclear medicine imaging called GATE (Geant4 Application for Tomographic Emission) through the GEANT4 Toolkit is also freely available, and a recent review describes its application to radionuclide dosimetry [83]. These platforms can account for radionuclide emissions and tissue density distributions, leading to extremely accurate dose distributions. Studies carried out comparing MC simulation packages to standard MIRD techniques show a negligible difference in absorbed energies between GATE and MIRD in a phantom over a range of monoenergetic photon energies (>50 keV) [84].

The power of these techniques can also be shown at the microscopic scale; Gulec et al. employed a MC simulation (using MCNPX) of a 3-D liver model, including various subunits of the hepatic anatomy [85]. They assessed the impact of the lower number of GMS per GBq (compared to RMS), showing that for both techniques, the liver dose for the compartmental and structural models are similar but that doses to the micro-anatomic structures can be more than 3 times larger than the liver dose for GMS over RMS. A similar MC study showed that the non-uniform trapping produced by GMS transport in a simulated arterial tree may explain their lower toxicity per Gy [41]. They showed a highly asymmetric spread of dose distribution, with 17% of lobules receiving < 40 Gy.

Owing to the effect whereby the necrotic tumour core is surrounded by activity as observed in liver explantations, a tumour necrosis model to correct the activity prescription for therapy evaluated using PENELOPE [86], separates the tumour into a sphere of necrosis surrounded by a uniform shell source of ^{90}Y activity. The results show that more beta particles escape the source region and deposit their energies in areas other than the tumour region, and the prescribed activity can be adjusted to take account of this geometrical correction. They further note that the prescribed activity is underestimated by more than 10% by not taking account of this correction.

Recent work has shown new advances in MC calculation algorithms, which accounts for tissue density heterogeneities, and allows a marked reduction in calculation time from 40 hours (10^8 histories using MCNP6) to 4 minutes using a "collapsed-cone" algorithm [87]. A comparison of mean dose for 6 phantoms and 2 clinical cases (1 ^{90}Y microspheres) showed a difference of <1% between the methods.

4.1.1 MC User-end codes

A user-end package called OEDIPE (based on MCNPX) developed at ISRN in France uses the patient's ^{90}Y Bremsstrahlung/PET and CT scans, and has recently applied their code to treatment optimization for hepatic metastases to patients treated with RMS [88]. They calculated the maximum injectable activity for the standard PM dosimetry, and also for an MC calculation using the same dosimetry considerations, as well as an MC calculation using DVH based dose constraints (i.e. only 50% of normal liver receiving a maximum of 30 Gy). Their results show that the maximum injectable activity can be substantially higher when compared to the activity calculation provided standard PM by 27% for the MC calculation using PM dosimetry considerations and by 40% when using DVH-based dose constraints.

Another well-established package called 3D-ID (developed in EGSnrc) has been extended to include radiobiological models derived from the linear quadratic equation, with BED (biologically equivalent dose) calculated for each voxel by estimating the clearance rate in each voxel using the radiobiological parameters α, β and μ (note α - radiosensitivity per unit dose, β - radiosensitivity per unit dose squared and μ - repair rate), and also an EUD value (effective uniform dose) for a particular user-defined volume. The code has been renamed 3D-RD [89] and recent validations were performed against a voxel S-value MIRD technique in a voxelized liver phantom with less than a 1% difference in absorbed dose [90]. More recently the same validation was performed to examine the effects of tissue density over 3 different radionuclide treatments (including ^{90}Y-RE) with differences of 0.8% in both D_T and D_{NL} [91].

4.2 Dose kernel convolution methods

Application of kernels in voxel-based geometries can be found in the computation of "Dose Voxel Kernels (DVK)" or "Voxel S-Values (VSV), which is input data suited for analytical convolution with voxel-based cumulated activity maps (i.e. from SPECT or PET imaging) as defined in MIRD Pamphlet 17 [92]. A VSV is defined as the mean absorbed dose to a target voxel per radioactive decay in a source voxel, both of which are contained in an infinite homogeneous tissue medium. The convolution of the S-value dose distribution (Gy MBq^{-1} s^{-1}) with the cumulated activity (MBq s) leads to a map of absorbed dose (Gy).

A comparison of MC codes (MCNP4C, EGSnrc and GEANT4) used to define the S-value matrix for β-emitters has been shown to affect dose distribution values by only a few percent [93]. MIRD pamphlet 17 originally produced VSVs for 3 voxel sizes and 5 isotopes although more recent work expanded these tables using simulations within the EGSnrc toolkit (and validated with PENELOPE and MCNP4c codes) with more isotopes and a larger range of voxel sizes more suited to modern scanners [94].

These VSV matrices are freely available at http://www.medphys.it/downloads.htm. Recent work has shown that provided VSVs are available for a high resolution voxel size from an MC simulation; VSVs for any lower resolution voxel size can easily be generated [95]. Compared to MC simulation for the larger voxels, this rescaling technique showed differences of 1.5% in scored energy deposition for ^{90}Y.

A similar approach whereby the fine VSV map was resampled to the same voxel size as the activity map was validated by comparisons to MC simulations (using 3D-RD) in a simulated hepatic tumour, showed a difference in absorbed dose of 0.33% for ^{90}Y [90]. A further clinical study by this group performed a comparison of the PM with a user-end code called VoxelDose for 10 HCC patients, showing mean relative differences of 1.5% for D_T and 4.4% for D_{NL}, noting that the entire process (after tissue segmentations) can be performed in 15 minutes [96].

User-end codes are easy to implement for ^{90}Y-RE, requiring only a convolution of the cumulated activity (from a single scan) with a VSV/DVK matrix to produce a 3D map of absorbed dose. A code called VoxelDose was validated in an abdominal phantom using ^{111}In with the dosimetry measured by TLDs [97]. They showed a range of errors from 3-62% in activity concentration dependent on the organ, which may be explained by the position of the TLDs. Another code called qDOSE is under development at the Royal Marsden (UK), which offers a specific version of the code aimed at dosimetry for ^{90}Y-RE using DVKs developed from EGSnrc environment [98]. Another recently developed user-end code called NUKDOS performs VSV dosimetry and has been validated against OLINDA and other in-house codes in peptide receptor radionuclide therapy (PRRT) [99].

As S-values are defined in a certain medium, the technique does not account for tissue in homogeneities. Assumptions can be made that heterogeneities do not induce significant errors with self-dose to the liver due to its size and composition. It has also been noted that if tissue heterogeneities cannot be ignored (i.e. for cross-dose calculation), a low number of histories can be used to generate the cross dose to the target organ using a direct MC methodology, and VSVs for the self-dose to the organ, and adding the results [90].

4.3 Local Deposition Method (LDM)

The Bremsstrahlung self-dose from an organ is very small compared to the beta radiation dose (0.2% of the total) [100]. Thus because of the average range of a β-particle and the low resolution of current clinical SPECT/PET imaging, ^{90}Y β-particles emitted within a single voxel range deposit energy locally (within the same voxel). Thus, the absorbed dose in each voxel can be determined by multiplying the activity concentration by a constant scalar factor. Recently published conversion factors allow these calculations [101].

As voxel sizes increase the differences between the LDM, VSV and direct MC methods are markedly reduced [102]. The LDM technique provides a fast and efficient method to transform activity concentration to absorbed dose and has been finding increasing clinical use, with a reported case study showing that after an infusion of RMS, a secondary infusion of RMS was used in order to provide a dose boost for the HCC to reach an absorbed dose of 120 Gy [103].

4.4 Dose Response Relationship

Despite a correlation between absorbed doses and treatment response and toxicity [9], all evidence supporting a dose response relationship from dosimetry in ^{90}Y-RE is based on either non-controlled prospective or retrospective studies.

A recent study reported on the lack of association between metastatic lesion based response (66 patients treated with RMS) and the overall MAA uptake (classified from 1 -no intratumoural uptake, to 4 -strong uptake) and that the metastatic response cannot be predicted by the degree of perfusion on ^{99m}Tc-MAA scanning while also showing no correlation between tumour response and catheter position [57]. This work shows conflicting results with other studies, and many recent letters have discussed these results in detail [59,73,104,105,106,107]. An important conclusion of these discussions is that in dosimetry comparisons of ^{90}Y-RE, consideration should be given to the type of microsphere, quantification method, tumour type and the method of response assessment. Further noted is that large-scale dosimetry comparison study of MAA data and ^{90}Y-MS imaging for the same set of patients is lacking [66].

Other ^{90}Y-RE studies treating HCC have shown a significant dose response relationship with predictive MAA imaging. In a study of 36 HCC patients treated with GMS, a strong correlation was noted between absorbed dose and tumour response (EASL criteria) and also with overall survival (OS). They determined a threshold dose of 205 Gy, which enabled a response prediction with 91% accuracy and 100% sensitivity [108]. Using this threshold in a cohort of 71 patients, the group detailed 17 patients who underwent treatment intensification to achieve D_T > 205 Gy while maintaining D_{NL} <120 Gy [109]. They show an OS of 11.5 months and 23.2 months for D_T < 205 Gy and > 205 Gy respectively. Similarly, a recent study of 52 HCC patients treated with GMS showed that a threshold D_T of 500 Gy was successful in predicting objective responses (via EASL criteria) in their cohort [110].

In an effort to counteract partial volume effects, they also excluded lesions < 3 cc (approximately 1.8 cm diameter) because of a 20% underestimation of activity for a 1.8 cm diameter sphere at a contrast ratio of 4:1 in a previous phantom study [47]. A recent study showed a correlation between D_T >100 Gy and survival in 18 HCC patients treated with GMS [76], as shown in Figure 3. Treating 25 patients with liver metastases with RMS and using a dual tracer (both pre-treatment ^{99m}Tc) partition model technique, a correlation between D_T and OS with a threshold dose of 55 Gy (32.8 months vs 7.2 months) was noted [111].

MAA distributions of 39 liver lesions and an LDM technique was used to show correlation between D_T and metabolic response by FDG PET [112]. Similarly, a mean D_T for 30 tumours using Bremsstrahlung imaging and ^{90}Y DPKs (Dose Point Kernels) showed that the percentage of tumour volume receiving >50 Gy significantly predicted a decrease in SUVmax (assessed with FDG-PET), and maximum D_T predicted a decrease in tumour metabolic activity.

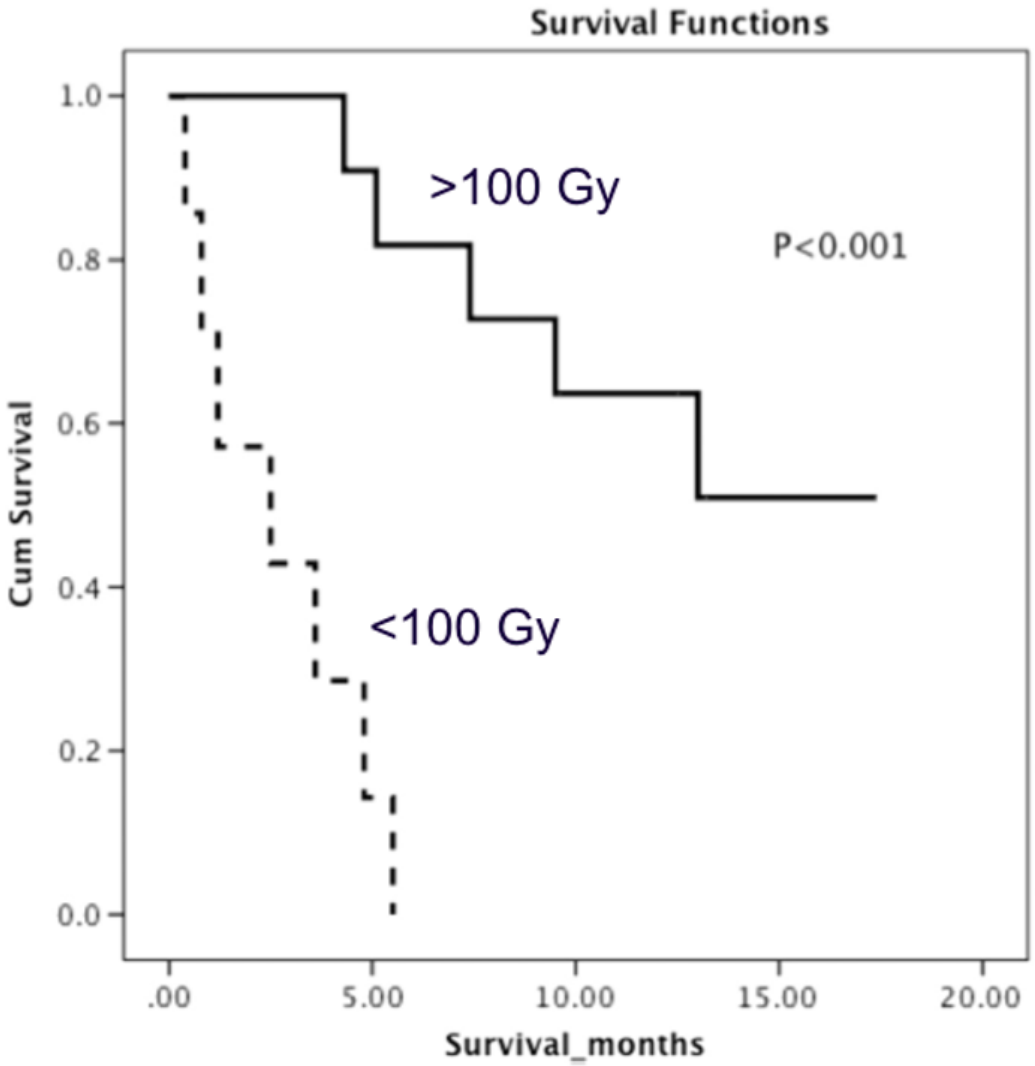

Figure 3. Example of overall survival curves with a tumour threshold of 100 Gy using GMS dosimetry. Reprinted with permission [76].

Although there has been much work on the radiobiological aspects of ^{90}Y-RE, convergence on a consensus approach to radiobiological model is required [113]. Currently, dosimetry calculations assume a single set of radiobiological values for cells making up a tumour or organ, although radiosensitivity of tissue components is known to be spatially dependent indicating that different radiobiological values may exist depending on the location within the tumour/organ [114]. A VSV method in 13 patients with liver metastases treated with RMS attempted to incorporate the EUD in place of D_T, and noted that α should be redefined for both normal liver and specific tumours before radiobiological quantities can be successfully employed [115]. Only recently has it been recommended that in any liver dosimetry analysis BED should be considered along with absorbed dose [47].

In a study of 73 patients with HCC, a TCP-NTCP radiobiological model and patient dosimetry calculated by DVK showed that the model predicted TCPs (complete or partial response) of 73% and 55% according to EASL and RECIST criteria using a mean D_T of 110 Gy [13]. They also observed (and predicted) toxicity of 34%, and calculated a BED50 of 93 Gy, close to the values of 72 Gy derived from EBRT [116].

Incorporating the microscale distribution of dose in a single hepatic lobule, the model was adapted and provided a method for computing NTCP as a function of microsphere activity and targeted liver volume [42].

A recent method to assess D_{NL} involves an injection of ^{99m}Tc-sulfur colloid post ^{99m}Tc-MAA SPECT, which allowed a determination of a threshold dose of 24.5 Gy to predict biochemical toxicity [111]. This method allows a more accurate assessment of the functional liver rather than relying on morphologic partition modelling, and further investigations are certainly warranted.

5. Emerging Directions

5.1 ^{90}Y PET Imaging

Although many groups have preliminarily investigated ^{90}Y PET imaging in terms of post-treatment imaging, it remains an underutilised modality of post-therapy imaging. Adequate visualisation can be achieved with a 20 minute per bed scan [117,118] and sensitivities of 0.11 cps/MBq in patients [119], 0.577 and 1 cps/MBq in phantom [117,120] have been reported. In a recent study, the optimal contrast for hot and cold spheres in a phantom was obtained with LYSO crystals and TOF technology [121]. Echoing this statement, a minimum detectable activity of 1 MBq/ml in a phantom was noted on a Siemens Biograph 40 for TOF reconstruction (3 MBq/ml in non-TOF) [122]. They also show the effect of PET image reconstruction on the activity recovered in a phantom, and that differences in activity on the order of ±20% can be obtained depending on the type of reconstruction performed.

High random to true ratios during imaging have shown that a positive mean bias of 3.3±6.4 Gy (averaged over 65 PET scans) can exist due to delayed random coincidence correction producing negative sinogram values, and these negative values being truncated prior to image reconstruction [123]. A physical and computer-simulated phantom with filled spheres and convoluted via a VSV technique showed approximately 9% difference (using PSF, recovery coefficients and TOF) in absorbed dose when compared to a known ground truth [124]. They noted that the use of the TOF in the reconstruction improved the accuracy of absorbed dose calculations for the simulated tumours with the lowest activities.

Many studies have shown an enhanced resolution of microsphere distribution around the tumour periphery with ^{90}Y-PET and also show potential to identify areas of sub-optimal microsphere deposition not detectable with gamma camera imaging [20,117], as shown in Figure 4. In a recent diagnostic image reporting study of target to non-target activity, ^{90}Y PET consistently outperformed ^{90}Y Bremsstrahlung [118].

Retrospective studies using PET dosimetry show that HCC lesion dosimetry using rescaled VSVs (using MCNP) showed a mean DT of 139.3 Gy and DNL of 33.8 Gy [120] and this work noted a dose of 287 Gy to the tumour periphery, and 70 Gy to the necrotic core.

Absorbed doses to 23 HCC patients with RMS using a LDM and 90Y PET, used DVHs to account for the heterogenous nature of microsphere distribution to determine a threshold of D70>100Gy for complete response of HCC [66]. Providing the first Gy-for-Gy comparison against MAA SPECT dosimetry for 7 patients, they showed an intraclass correlation of 0.97, in the cohort, with a maximum difference of up to 40% in DT. Similar work showed that in 64 patients with HCC treated with GMS and using VSVs that DNL was 93±33 Gy with on average V50 > 79 Gy and DT of 173±103 Gy [125].

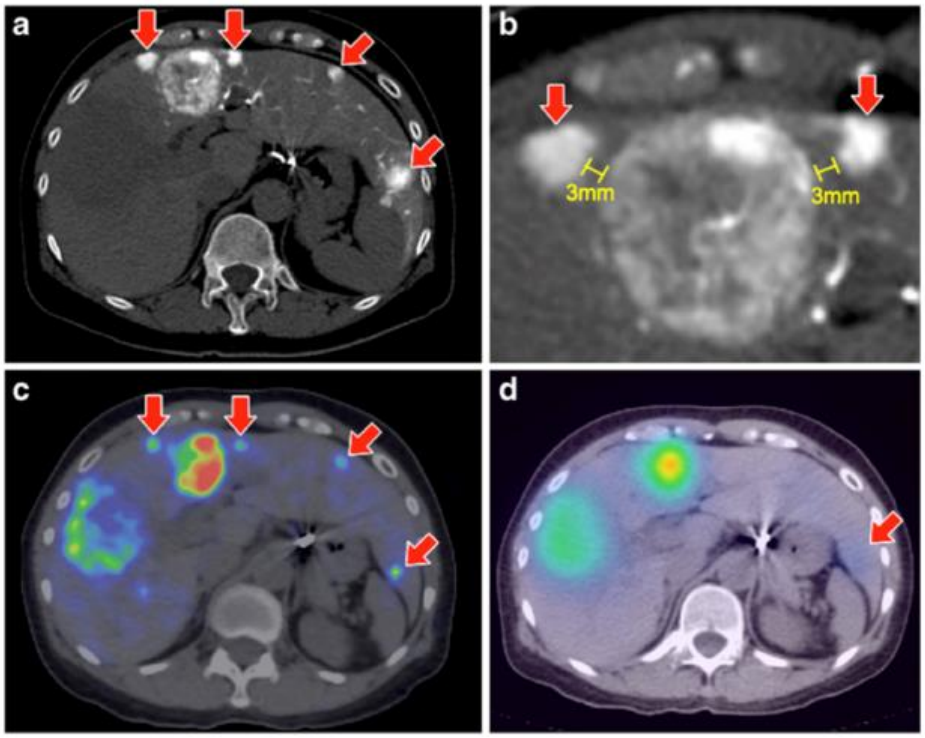

Figure 4. Comparison between ^{90}Y-PET (**c**) and ^{90}Y-Bremsstrahlung images (**d**) showing the superior resolution of PET in terms of highlighting further small tumours (red arrows) clearly observed in CT (**a** and **b**). Also observed is the necrotic core of the largest tumour towards the left of the image. Reproduced with permission [118].

Recent work used FLUKA to develop a DVK technique for PET-CT scans for 6 patients (3 GMS, 3 RMS) and used DVHs to show D_{70} in the range of 25-155 Gy for all patients, and a mean D_T of 71-311 Gy [126]. VSVs and PET were also used for 5 patients treated with RMS showing a range of D_T from 51-163 Gy. This work also calculated the BED and converted this to dose equivalent to delivery at 2 Gy/fraction, upon which limits for TCP and NTCP are published. They further showed that the differences in D_T using the PM from the MAA scan and those calculated from VSV PET-CT were in the range of -53.8% to +178.4%. The emerging role of quantitative PET-CT in ^{90}Y-RE is further developed in a recent review [127].

5.2 Preplanning with PET isotopes

Efforts have been made to supplant ^{99m}Tc-MAA imaging with microspheres labelled with a positron-emitting isotope, which would provide higher resolution imaging and enable improvements in PET predictive dosimetry.

Recent work has labelled RMS with ^{64}Cu, ^{86}Y and ^{89}Zr with efficiencies of >95% (although 80% for ^{89}Zr) [128]. ^{64}Cu was excluded due to leaching of Cu(II), and ^{86}Y as it emits photons detected in the PET imaging window. They showed good ^{89}Zr imaging characteristics in phantoms and a lower cost associated with production [129]. Given the comparable half-life of ^{89}Zr to ^{90}Y, the group then produced ^{18}F-based RMS [130]. They achieved a labelling efficiency of 95% and an *in vitro* stability study of >99%, showing histological analysis of microsphere distribution in the rabbit liver agreed with PET findings to within 3%. They showed, however, that 15% leaching occurred at 45 min post-injection, and thus it would prove difficult to provide accurate activity quantification using ^{18}F microspheres. A recent review highlighted the issues inherent with "non-pure" positron emitters such as ^{86}Y, ^{124}I, ^{94m}Tc because of prompt gamma rays emitted in the PET acquisition window, and also higher energy gamma rays that may scatter into the same window [131]. Significant corrections are required in order to accurately image these isotopes especially for quantitative 3D PET where the potential for spurious coincidence contamination is much increased. Other efforts into using biodegradable Chitosan glycol MS labelled to ^{68}Ga have been developed in preclinical models [132], although no clinical results are yet available.

5.3 Other Treatment Isotopes

The Utrecht group have successfully produced poly (L-lactic acid) microspheres loaded with holmium-166 (^{166}Ho-PLLA)[133], and proposed a phase 1 trial (called HEPAR) to treat patients with liver metastases in 2010 [134], with a dose-escalation protocol of 20, 40, 60 and 80 Gy using MIRD macrodosimetry (achieved with varying GBq/kg of liver weight). The properties of the microspheres are shown in Table 3. A gamma emission at 81 keV enables SPECT imaging, and the spheres are biodegradable, meaning no permanent embolization occurs. GATE simulations of a liver tumour and gamma camera details a better localization potential of ^{166}Ho SPECT than ^{90}Y Bremsstrahlung images [135].

In a porcine model, the group showed good correlation of biodistribution of scout doses (250 MBq) and treatment doses of 166Ho-PLLA [136]. The results of the HEPAR trial (15 patients) [137], show the maximum tolerated radiation dose to the whole liver for the cohort to be 60 Gy (toxicity occurred in 2 of 3 patients receiving 80 Gy), and proposed this as an endpoint for a phase 2 trial.

As 166Ho-PLLA microspheres are paramagnetic, they can also be observed on MR imaging via the microsphere induced change in relaxation rates per mg/ml from a baseline scan acquired before therapy [137]. Activity quantitation was achieved using the specific activity of the spheres, and a good correlation (R2=0.91) was shown between MR and SPECT calculated dosimetry to liver segments

http://dx.doi.org/10.17229/jdit.2015-0428-016

determined from a convolution with a DVK [138]. From their work, administration under real-time MR imaging may be a technical possibility.

Name	^{166}Ho-PLLA-MS (UMC Utrecht)
Radioisotope	^{166}Ho
Isotope location	Incorporated into matrix
β emission (MeV)	1.77 (49%), 1.85 (50%)
ϒ emission (keV)	80.6 (6.7%)
Matrix material	PLLA
Density (g/mL)	1.4
Av Diameter	30±5
Number of particles	33x10^6
Bq per sphere	≤450
Embolic effect	Mild-moderate
Available Activity	Any
Endpoint	Target Dose

Table 3. Properties of ^{166}Ho-PLLA microspheres [134].

^{142}Pr has also been identified as another possible choice for RE ($t_{½}$ =19.12 hrs, $E_{\beta max}$= 2.16 MeV, E_{γ}=1.57 MeV), and a simulation study compared dose distributions of ^{142}Pr and ^{90}Y within a hepatic tumour and blood vessels using MCNPX [139]. They showed a higher BED of 301 Gy for ^{142}Pr against 195 Gy for ^{90}Y. Although this represents very early work, it may be an emerging isotope for future trials.

5.4 Delivery of Spheres

A recent study has shown that D_{NL} can be reduced by the use of temporary degradable starch microspheres (DSM), which lead to temporary redistribution of blood flow away from the embolised tissue [77]. The technique was applied in cases where catheter repositioning was not possible due to location of metastatic deposits for 5 patients and MAA SPECT before and after DSM application showed further selectivity of the tumour, while sparing normal liver tissue. There were no adverse events or evidence of REILD on follow-up.

A recent technical development in the catheterization system (called the Surefire Infusion System) provides a way to bypass coil embolization. During the RE procedure, retrograde passage of embolic particles is prohibited by an expandable tip, which opens under retrograde flow conditions and collapses under forward flow. This technique has so far been performed on small cohorts of patients, and allowing treatment on a patient who would otherwise not have been treated with the conventional microcatheter technique [140,141]. The catheter results in a reduction in procedure time and may represent the next step in standard RE treatment.

5.5 "Extended shelf-life" Technique

A method to balance the desired embolic load with microsphere activity can be achieved by taking advantage of the long shelf-life of GMS (12 days) [48]. The "extended shelf-life" technique administered an average increase of 111% in embolic load (of lower specific activity 266±38 Bq per sphere) to a cohort of 50 patients, almost doubling the required number of GMS to achieve 100 Gy to normal tissue [37]. Their results show better tumour coverage (perhaps due to an increased number of clusters of spheres) and EASL response rates in patients with extensive tumour burden or marked tumour hypervascularity. In a follow-up study of 134 patients, they showed similar response rates with the addition of 84 patients and also validating the safety and efficacy of the technique [142].

6. Conclusions

The shift towards personalised radionuclide therapy is an inevitable trend. However dose-response effects in terms of toxicity to normal organs and survival must first be proven as part of a randomised clinical trial. Noting that techniques in ^{90}Y-RE dosimetry are well advanced, but confidence in the techniques needs to increase, Kao states "the major barrier to the routine application of predictive dosimetry for ^{90}Y-RE is no longer the state of the art but rather the state of our hearts" [143] indicating that while many of the techniques for predictive and retrospective dosimetry are already available, the effort involved in employing them, the reliability of the results provided by them, and more crucially, trusting their accuracy and precision, is not a trivial undertaking. This lack of confidence in dosimetry is potentially a consequence of current limitations in the entire therapeutic procedure, ranging from MAA-MS imaging mismatches, poor imaging resolution, and quantification errors and also fundamental errors associated with MS activity measurements in ion chambers.

As mentioned in this review, studies performing dose escalation based on partition model, MIRD techniques or BSA dosimetry are making important clinical decisions based on dosimetry results, showing belief in the methodology. Thus great attention to detail should be placed on the radiobiological considerations and fundamental quantification methodology to allow accurate absorbed dose determination. The spatial and temporal variation of dose rate will have varying radiobiological effects on tumour control and normal liver sparing and due to the dose gradient, each voxel of the tumour and healthy liver receives a different absorbed dose at a different time. Current efforts into modelling at the microscopic scale will hopefully help address these issues.

Noting that many published papers fail to describe their dosimetry methodology, the EANM Dosimetry group have published guidelines and a documentation checklist of all the relevant parameters for reporting of the parameters and procedures involved [144], which should help to enable results and techniques to be compared cross-site. This standardisation becomes important as ^{90}Y-RE begins to be applied to tumours in other body sites such as lung metastases through the bronchial artery [145].

The ongoing MetroMRT http://projects.npl.co.uk/metromrt/ project aims to address some of the fundamental issues highlighted in this review, such as standardisation of microsphere calibration in an ion chamber and standardised quantification procedures. Specific work packages were created to examine procedures of ^{90}Y-RE [146], and the expected outcomes of the project will be recommendations for standard practice. The French project DosiTest www.dositest.fr aims to evaluate the impact of the various steps that contribute to the realization of a dosimetric study by the use of a virtual multi-centre intercomparison based on Monte-Carlo modelling. They employ scintigraphic images generated at a core lab using GATE, with users analysing them with their own dosimetry protocol [147]. The aim is to evaluate bias of certain dosimetry approaches and to propose a reference methodology applicable in a clinical setting.

The use of patient-specific Monte Carlo techniques has increased rapidly as the computational requirements are more easily met. Platforms such as GATE, EGS and MCNP are being increasingly employed for their versatility for using patient specific scans to produce reference absorbed dose calculations. A typical patient-specific calculation can be performed using GATE in 16 hours (with 2% uncertainty), within the conventional pretherapeutic imaging to therapy time [83]. As these platforms and applications advance, further user end codes are expected to be available which may help to remove the barrier of detailed technical knowledge of the programs and concentrated resources required to perform these simulations in a clinical setting.

The emerging techniques described in this work are aiming to address certain deficiencies in the current technique, such as ^{90}Y-PET, which can provide high resolution imaging and does not require considerable corrections to the imaging process in order to provide quantitative values. Ideally this would be preceded by a PET pre-therapy scan of similar resolution for dosimetry purposes, which is not yet clinically available. Other efforts such as the use of ^{166}Ho-PLLA make SPECT imaging more reliable and more easily quantifiable due to the gamma ray emission, and its use in pre-therapy imaging ensures that the imaging discordance as a result of particulate differences should not be an issue.

Reducing the time the patient spends in the clinic is also an important factor for advancement of the therapy. A recent proof of concept study evaluated the potential for performing cone-beam CT, angiography with pretherapeutic embolisations, planar MAA imaging, LSF determination, dosimetry calculations (from MAA images) and GMS implantation as a single-session treatment as an outpatient procedure [148]. 14 patients underwent the modified procedure, and the average procedure time was 2.7 ± 0.72 hours (maximum of 4 hours). Although no post-therapy imaging is performed, it shows great potential for future applications in terms of reduced time, cost and resources but also requiring an increase in coordination between the relevant multidisciplinary teams.

Conflicts of Interest

The author reports no conflicts of interest

Acknowledgements

The author acknowledges financial support from the Department of Health via the National Institute for Health Research (NIHR) comprehensive Biomedical Research Centre award to Guy's & St Thomas' NHS Foundation Trust in partnership with King's College London and King's College Hospital NHS Foundation Trust.

References

Key Article References: 9, 12, 20, 42, 58, 66, 101, 110, 137, 144

[1] Ferlay J, Soerjomataram I, Ervik M, et al. GLOBOCAN 2012 v1.0, Cancer Incidence and Mortality Worldwide: IARC CancerBase No. 11 [Internet]. Lyon, France: International Agency for Research on Cancer; 2013. [Reference Source]

[2] (CRUK) CRU. Cancer Statistics of Liver Cancer. 2014. [Reference Source]

[3] El-Serag H. Hepatocellular carcinoma. *N Engl J Med*. 2011; 365: 1118-1127. [CrossRef] [PubMed Abstract]

[4] Misiakos EP, Karidis NP, Kouraklis G. Current treatment for colorectal liver metastases. *World J Gastroenterol*. 2011; 17(36): 4067-4075. [CrossRef] [PubMed Abstract]

[5] Kennedy A. Radioembolization of hepatic tumors. *J Gastrointest Oncol.* 2014; 5(3): 178-189. [Reference Source] [PubMed Abstract]

[6] Popescu I, Alexandrescu ST. Surgical options for initially unresectable colorectal liver metastases. *HPB Surg*. 2012; 2012: 454026. [CrossRef] [PubMed Abstract]

[7] Biermann HR, Byron RL, Kelley KH, Grady A. Studies on the blood supply of tumors in man. III. Vascular patterns of the liver by hepatic arteriography *in vivo*. *J Natl Cancer Institute*. 1951; 12(1). 107-131. [PubMed Abstract]

[8] Flux GD, Bardies M, Lassmann M. Biting the magic bullet: celebrating a decade of the EANM Dosimetry Committee. *Eur J Nucl Med Mol Imaging*. 2014; 41: 1-3. [CrossRef] [PubMed Abstract]

[9] Strigari L, Konijnenberg M, Chiesa C, et al. The evidence base for the use of internal dosimetry in the clinical practice of molecular radiotherapy. *Eur J Nucl Med Mol Imaging.* 2014; 41(10): 1976-1988. [CrossRef] [PubMed Abstract]

[10] Brans B, Bodei L, Giammarile F, et al. Clinical radionuclide therapy dosimetry: the quest for the "Holy Gray". *Eur J Nucl Med Mol Imaging*. 2007; 34(5): 772-786. [CrossRef] [PubMed Abstract]

[11] Sgouros G, Hobbs RF. Dosimetry for radiopharmaceutical therapy. *Semin Nucl Med*. 2014; 44(3): 172-178. [CrossRef] [PubMed Abstract]

[12] Bardiès M, Buvat I. Dosimetry in nuclear medicine therapy: what are the specifics in image quantification for dosimetry? *Q J Nucl Med Mol Imaging*. 2011; 55(1): 5-20. [Reference Source] [PubMed Abstract]

[13] Strigari L, Sciuto R, Rea S, et al. Efficacy and toxicity related to treatment of hepatocellular carcinoma with ^{90}Y-SIR spheres: radiobiologic considerations. *J Nucl Med*. 2010; 51(9): 1377-1385.
[CrossRef] [PubMed Abstract]

[14] Thomas SR. Options for Radionuclide Therapy: From Fixed Activity to Patient-Specific Treatment Planning. *Cancer Biotherm Radiopharm*. 2002; 17(1): 71-82.
[CrossRef] [PubMed Abstract]

[15] Kennedy AS, Nutting C, Coldwell D, Gaiser J, Drachenberg C. Pathologic response and microdosimetry of (90)Y microspheres in man: review of four explanted whole livers. *Int J Radiat Oncol Biol Phys*. 2004; 60(5): 1552-1563.
[Reference Source] [PubMed Abstract]

[16] Murthy R, Nunez R, Szklaruk F, et al. Yttrium-90 Microsphere Therapy for Hepatic Malignancy: Devices, Indications, Technical Considerations, and Potential Complications. *Radiographics*. 2005; 25 (Suppl 1): S41-55.
[Reference Source] [PubMed Abstract]

[17] Uliel L, Royal HD, Darcy MD, Zuckerman DA, Sharma A, Saad NE. From the angio suite to the gamma-camera: vascular mapping and ^{99m}Tc-MAA hepatic perfusion imaging before liver radioembolization - a comprehensive pictorial review. *J Nucl Med.* 2012; 53(11): 1736-1747.
[Reference Source] [PubMed Abstract]

[18] Garin E, Rolland Y, Lenoir L, et al. Utility of Quantitative Tc-MAA SPECT/CT for yttrium-Labelled Microsphere Treatment Planning: Calculating Vascularized Hepatic Volume and Dosimetric Approach. *International Journal of Molecular Imaging.* 2011; 2011: 398051.
[Reference Source] [PubMed Abstract]

[19] Kao YH, Hock Tan AE, Burgmans MC, et al. Image-guided personalized predictive dosimetry by artery-specific SPECT/CT partition modeling for safe and effective ^{90}Y radioembolization. *J Nucl Med*. 2012; 53(4): 559-566.
[CrossRef] [PubMed Abstract]

[20] Kao YH, Tan EH, Ng CE, Goh SW. Yttrium-90 Time-of-Flight PET/CT Is Superior to Bremsstrahlung SPECT/CT for Postradioembolization Imaging of Microsphere Biodistribution. *Clin Nucl Med*. 2011; 36(12): e186-e187.
[Reference Source] [PubMed Abstract]

[21] Hamami ME, Poeppel TD, Muller S, et al. SPECT/CT with ^{99m}Tc-MAA in radioembolization with ^{90}Y microspheres in patients with hepatocellular cancer. *J Nucl Med*. 2009; 50(5): 688-692.
[CrossRef] [PubMed Abstract]

[22] Ahmadzadehfar H, Sabet A, Biermann K, et al. The significance of ^{99m}Tc-MAA SPECT/CT liver perfusion imaging in treatment planning for ^{90}Y-microsphere selective internal radiation treatment. *J Nucl Med*. 2010; 51(8): 1206-1212.
[CrossRef] [PubMed Abstract]

[23] Kao YH, Tan EH, Teo TK, Ng CE, Goh SW. Imaging discordance between hepatic angiography versus Tc-99m-MAA SPECT/CT: a case series, technical discussion and clinical implications. *Ann Nucl Med.* 2011; 25(9): 669-676.
[CrossRef] [PubMed Abstract]

[24] Gray B, Van Hazel G, Hope M, et al. Randomised trial of SIR-Spheres® plus chemotherapy vs. chemotherapy alone for treating patients with liver metastases from primary large bowel cancer. *Ann Oncol.* 2001; 12: 1711-1720.
[Reference Source][PubMed Abstract]

[25] Kennedy A, Nag S, Salem R, et al. Recommendations for radioembolization of hepatic malignancies using yttrium-90 microsphere brachytherapy: a consensus panel report from the radioembolization brachytherapy oncology consortium. *Int J Radiat Oncol Biol Phys*. 2007; 68(1): 13-23.
[CrossRef] [PubMed Abstract]

[26] Kennedy AS, McNeillie P, Dezarn WA, et al. Treatment parameters and outcome in 680 treatments of internal radiation with resin ^{90}Y-microspheres for unresectable hepatic tumors. *Int J Radiat Oncol Biol Phys.* 2009; 74(5): 1494-1500.
[CrossRef] [PubMed Abstract]

[27] Leung TW, Lau WY, Ho SKW, et al. Radiation pneumonitis after selective internal radiation treatment with intraarterial ^{90}Yttrium-microspheres for inoperable hepatic tumors. *Int J Radiat Oncol Biol Phys.* 1995; 33(4): 919-924.
[CrossRef] [PubMed Abstract]

[28] Giammarile F, Bodei L, Chiesa C, et al. EANM procedure guideline for the treatment of liver cancer and liver metastases with intra-arterial radioactive compounds. *Eur J Nucl Med Mol Imaging.* 2011; 38(7): 1393-1406.
[Reference Source] [PubMed Abstract]

[29] Lau WY, Kennedy AS, Kim YH, et al. Patient selection and activity planning guide for selective internal radiotherapy with yttrium-90 resin microspheres. *Int J Radiat Oncol Biol Phys.* 2012; 82(1): 401-407.
[CrossRef] [PubMed Abstract]

[30] About SIR-Spheres microspheres.
[Reference Source]

[31] Stabin M. Nuclear medicine dosimetry. *Phys Med Biol.* 2006; 51(13): R187-202.
[CrossRef] [PubMed Abstract]

[32] Gulec S, Mesoloras G, Stabin M. Dosimetric Techniques in ^{90}Y-Microsphere Therapy of Liver Cancer: The MIRD Equations for Dose Calculations. *J Nucl Med*. 2006; 47(7): 1209-1211.
[Reference Source] [PubMed Abstract]

[33] Ho S, Lau WY, Leung TWT, Chan M, Johnson PJ, Li AKC. Clinical evaluation of the partition model for estimating radiation doses from yttrium-90 microspheres in the treatment of hepatic cancer. *Eur J Nucl Med*. 1997; 24(3): 293-298.
[CrossRef] [PubMed Abstract]

[34] Lau WY, Leung TW, Ho S, et al. Treatment of inoperable hepatocellular carcinoma with intrahepatic arterial yttrium-90 microspheres: a phase I and II study. *Br J Cancer*. 1994; 70: 994-999.
[CrossRef] [PubMed Abstract]

[35] Garin E, Rolland Y, Boucher E. Pre-therapeutic dosimetry evaluation and selective internal radiation therapy of hepatocellular carcinoma using yttrium-90-loaded microspheres. *J Hepatol.* 2013; 58(5): 1055-1056.
[Reference Source] [PubMed Abstract]

[36] Sangro B, Inarrairaegui M, Bilbao JI. Reply to: "Pre-therapeutic dosimetry evaluation and selective internal radiation therapy of hepatocellular carcinoma using yttrium-90-loaded microspheres". *J Hepatol.* 2013; 58(5): 1056-1057.
[CrossRef] [PubMed Abstract]

[37] Lewandowski RJ, Riaz A, Ryu RK, et al. Optimization of radioembolic effect with extended-shelf-life yttrium-90 microspheres: results from a pilot study. *J Vasc Interv Radiol.* 2009; 20(12): 1557-1563.
[CrossRef] [PubMed Abstract]

[38] Sangro B, Inarrairaegui M, Bilbao JI. Radioembolization for hepatocellular carcinoma. *J Hepatol.* 2012; 56(2): 464-473.
[CrossRef] [PubMed Abstract]

[39] Rhee TK, Lewandowski RJ, Liu DM, et al. ^{90}Y Radioembolization for metastatic neuroendocrine liver tumors: preliminary results from a multi-institutional experience. *Ann Surg.* 2008; 247(6): 1029-1035.
[Reference Source] [PubMed Abstract]

[40] Paxton AB, Davis SD, Dewerd LA. Determining the effects of microsphere and surrounding material composition on ^{90}Y dose kernels using egsnrc and mcnp5. *Med Phys*. 2012; 39: 1424-1434.
[Reference Source] [PubMed Abstract]

[41] Walrand S, Hesse M, Chiesa C, Lhommel R, Jamar F. The low hepatic toxicity per Gray of ^{90}Y glass microspheres is linked to their transport in the arterial tree favoring a nonuniform trapping as observed in posttherapy PET imaging. *J Nucl Med*. 2014; 55(1): 135-140.
[CrossRef] [PubMed Abstract]

[42] Walrand S, Hesse M, Jamar F, Lhommel R. A Hepatic Dose-Toxicity Model Opening the Way Toward Individualized Radioembolization Planning. *J Nucl Med*. 2014; 55(8): 1317-1322.
[CrossRef] [PubMed Abstract]

[43] Goin JE, Salem R, Carr BI, et al. Treatment of unresectable hepatocellular carcinoma with intrahepatic Yttrium 90 microspheres: Factors associated with liver toxicities. *J Vasc Interv Radiol.* 2005; 16(2): 205-213.
[CrossRef] [PubMed Abstract]

[44] Chiesa C, Mira M, Maccauro M, et al. A dosimetric treatment planning strategy in radioembolization of hepatocarcinoma with ^{90}Y glass microspheres. *Q J Nucl Med Mol Imaging*. 2012; 56(6): 503-508.
[Reference Source] [PubMed Abstract]

[45] Sangro B, Gil-Alzugaray B, Rodriguez J, et al. Liver disease induced by radioembolization of liver tumors: description and possible risk factors. *Cancer.* 2008; 112(7): 1538-1546.
[CrossRef] [PubMed Abstract]

[46] Gulec SA, Mesoloras G, Dezarn WA, McNeillie P, Kennedy AS. Safety and efficacy of Y-90 microsphere treatment in patients with primary and metastatic liver cancer: the tumor selectivity of the treatment as a function of tumor to liver flow ratio. *J Transl Med*. 2007; 5: 15.
[CrossRef] [PubMed Abstract]

[47] Chiesa C, Maccauro M, Romito R, et al. Need, feasibility and convenience of dosimetric treatment planning in liver selective internal radiation therapy with ^{90}Y microspheres: the experience of the National Tumor Institute of Milan. *Q J Nucl Med Mol Imaging*. 2011; 55(2): 168-197.
[CrossRef] [PubMed Abstract]

[48] Spreafico C, Maccauro M, Mazzaferro V, Chiesa C. The dosimetric importance of the number of ^{90}Y microspheres in liver transarterial radioembolization (TARE). *Eur J Nucl Med Mol Imaging.* 2014; 41(4): 634-638.
[CrossRef] [PubMed Abstract]

[49] DeZarn WA, Cessna JT, DeWerd LA, et al. Recommendations of the American Association of Physicists in Medicine on dosimetry, imaging, and quality assurance procedures for ^{90}Y microsphere brachytherapy in the treatment of hepatic malignancies. *Med Phys*. 2011; 38(8): 4824-4845.
[CrossRef] [PubMed Abstract]

[50] DeZarn WA, Kennedy AS. Resin ^{90}Y microsphere activity measurements for liver brachytherapy. *Med Phys*. 2007; 34(6): 1896-1900.
[Reference Source] [PubMed Abstract]

[51] Mo L, Avci B, James D, et al. Development of activity standard for ^{90}Y microspheres. *Appl Radiat Isot*. 2005; 63(2): 193-199.
[CrossRef] [PubMed Abstract]

[52] Selwyn R, Micka J, DeWerd L, Nickles R, Thomadsen B. Technical note: The calibration of Y 90 - labeled SIR - Spheres using a nondestructive spectroscopic assay. *Med Phys*. 2008; 35(4): 1278-1279.
[CrossRef] [PubMed Abstract]

[53] Kennedy A, Dezarn W, Weiss A. Patient Specific 3D Image-Based Radiation Dose Estimates for ^{90}Y Microsphere Hepatic Radioembolization in Metastatic Tumors. *J Nucl Med Radiat Ther*. 2011; 2:111.
[CrossRef]

[54] Lam MG, Louie JD, Abdelmaksoud MH, Fisher GA, Cho-Phan CD, Sze DY. Limitations of body surface area-based activity calculation for radioembolization of hepatic metastases in colorectal cancer. *J Vasc Interv Radiol.* 2014; 25(7): 1085-1093.
[CrossRef] [PubMed Abstract]

[55] Bernardini M, Smadja C, Farragi M, et al. Liver Selective Internal Radiation Therapy with ^{90}Y resin microspheres: Comparison between pre-treatment activity calculation methods. *Physica Medica: European Journal of Medical Physics.* 2014; 30(7): 752-764.
[CrossRef] [PubMed Abstract]

[56] Lau WY, Lai EC, Leung TW. Current role of selective internal irradiation with yttrium-90 microspheres in the management of hepatocellular carcinoma: a systematic review. *Int J Radiat Oncol Biol Phys*. 2011; 81(2): 460-467. [CrossRef] [PubMed Abstract]

[57] Ulrich G, Dudeck O, Furth C, et al. Predictive value of intratumoral ^{99m}Tc-macroaggregated albumin uptake in patients with colorectal liver metastases scheduled for radioembolization with ^{90}Y-microspheres. *J Nucl Med*. 2013; 54(4): 516-522. [CrossRef] [PubMed Abstract]

[58] Wondergem M, Smits ML, Elschot M, et al. ^{99m}Tc-macroaggregated albumin poorly predicts the intrahepatic distribution of ^{90}Y resin microspheres in hepatic radioembolization. *J Nucl Med.* 2013; 54(8): 1294-1301. [CrossRef] [PubMed Abstract]

[59] Amthauer H, Ulrich G, Grosser OS, Ricke J. Reply: Pretreatment Dosimetry in HCC Radioembolization with ^{90}Y Glass Microspheres Cannot Be Invalidated with a Bare Visual Evaluation of ^{99m}Tc-MAA Uptake of Colorectal Metastases Treated with Resin Microspheres. *J Nucl Med.* 2014; 55(7): 1216-1218. [CrossRef] [PubMed Abstract]

[60] Kao YH, Tan EH, Ng CE, Goh SW. Clinical implications of the body surface area method versus partition model dosimetry for yttrium-90 radioembolization using resin microspheres: a technical review. *Ann Nucl Med*. 2011; 25(7): 455-461. [CrossRef] [PubMed Abstract]

[61] Lambert B, Mertens J, Sturm EJ, Stienaers S, Defreyne L, D'Asseler Y. ^{99m}Tc-labelled macroaggregated albumin (MAA) scintigraphy for planning treatment with ^{90}Y microspheres. *Eur J Nucl Med Mol Imaging*. 2010; 37(12): 2328-2333. [CrossRef] [PubMed Abstract]

[62] De Gersem R, Maleux G, Vanbilloen H, et al. Influence of Time Delay on the Estimated Lung Shunt Fraction on ^{99m}Tc-Labeled MAA Scintigraphy for ^{90}Y Microsphere Treatment Planning. *Clin Nucl Med*. 2013; 38(12): 940-942. [Reference Source] [PubMed Abstract]

[63] O' Doherty J, Scuffham J, Hinton P. The importance of scatter correction for the assessment of lung shunting prior to yttrium-90 radioembolization therapy. *Nucl Med Commun*. 2011; 32(7): 628-634. [Reference Source] [PubMed Abstract]

[64] Heard S. Bremsstrahlung imaging for radionuclide therapy. London: University of London; 2008. [Reference Source]

[65] Minarik D, Sjogreen Gleisner K, Ljungberg M. Evaluation of quantitative (90)Y SPECT based on experimental phantom studies. *Phys Med Biol*. 2008; 53(20): 5689-5703. [Reference Source] [PubMed Abstract]

[66] Kao YH, Steinberg J, Tay YS, et al. Post-radioembolization yttrium-90 PET/CT - part 2: dose-response and tumor predictive dosimetry for resin microspheres. *EJNMMI Res.* 2013; 3: 57. [CrossRef] [PubMed Abstract]

[67] Rong X, Du Y, Ljungberg M, Rault E, Vandenberghe S, Frey EC. Development and evaluation of an improved quantitative ^{90}Y bremsstrahlung SPECT method. *Med Phys*. 2012; 39(5): 2346-2358. [Reference Source] [PubMed Abstract]

[68] Elschot M, Lam MG, van den Bosch MA, Viergever MA, de Jong HW. Quantitative Monte Carlo-based ^{90}Y SPECT reconstruction. *J Nucl Med.* 2013; 54(9): 1557-1563. [CrossRef] [PubMed Abstract]

[69] Dewaraja YK, Frey EC, Sgouros G, et al. MIRD pamphlet No. 23: quantitative SPECT for patient-specific 3-dimensional dosimetry in internal radionuclide therapy. *J Nucl Med*. 2012; 53(8): 1310-1325. [CrossRef] [PubMed Abstract]

[70] Walrand S, Hesse M, Demonceau G, Pauwels S, Jamar F. Yttrium-90-labeled microsphere tracking during liver selective internal radiotherapy by bremsstrahlung pinhole SPECT: feasibility study and evaluation in an abdominal phantom. *EJNMMI Res*. 2011; 1: 32.
[CrossRef] [PubMed Abstract]

[71] Maccauro M, Lorenzoni A, Boni G, et al. Multiagent imaging of liver tumors with reference to intra-arterial radioembolization. *Clinical and Translational Imaging*. 2013; 1(6): 423-432.
[CrossRef]

[72] Van de Wiele C, Maes A, Brugman E, et al. SIRT of liver metastases: physiological and pathophysiological considerations. *Eur J Nucl Med Mol Imaging*. 2012; 39(10): 1646-1655.
[Reference Source] [PubMed Abstract]

[73] Chiesa C, Lambert B, Maccauro M, et al. Pretreatment Dosimetry in HCC Radioembolization with ^{90}Y Glass Microspheres Cannot Be Invalidated with a Bare Visual Evaluation of ^{99m}Tc-MAA Uptake of Colorectal Metastases Treated with Resin Microspheres. *J Nucl Med.* 2014; 55(7): 1215-1216.
[CrossRef] [PubMed Abstract]

[74] Knešaurek K, Machac J, Muzinic M, DaCosta M, Zhang Z, Heiba S. Quantitative comparison of Yttrium-90 (90Y)-microspheres and Technetium-99m (99mTc)-macroaggregated albumin SPECT images for lanning ^{90}Y therapy of liver cancer. *Technol Cancer Res Treat*. 2010; 9(3): 253-262.
[Reference Source] [PubMed Abstract]

[75] Jiang M, Fischman A, Nowakowski FS. Segmental Perfusion Differences on Paired Tc-99m Macroaggregated Albumin (MAA) Hepatic Perfusion Imaging and Yttrium-90 (Y-90) Bremsstrahlung Imaging Studies in SIR-Sphere Radioembolization: Associations with Angiography. *J Nucl Med Radiat Ther*. 2012; 3: 122.
[Reference Source]

[76] Kokabi N, Galt JR, Xing M, et al. A simple method for estimating dose delivered to hepatocellular carcinoma after yttrium-90 glass-based radioembolization therapy: preliminary results of a proof of concept study. *J Vasc Interv Radiol*. 2014; 25(2): 277-287.
[CrossRef] [PubMed Abstract]

[77] Meyer C, Pieper CC, Ezziddin S, Wilhelm KE, Schild HH, Ahmadzadehfar H. Feasibility of temporary protective embolization of normal liver tissue using degradable starch microspheres during radioembolization of liver tumours. *Eur J Nucl Med Mol Imaging.* 2014; 41(2): 231-237.
[CrossRef] [PubMed Abstract]

[78] Basciano CA, Kleinstreuer C, S. Kennedy A. Computational Fluid Dynamics Modeling of ^{90}Y Microspheres in Human Hepatic Tumors. *J Nucl Med Radiat Ther*. 2011; 2:112.
[Reference Source]

[79] Kennedy AS, Kleinstreuer C, Basciano CA, Dezarn WA. Computer modeling of yttrium-90-microsphere transport in the hepatic arterial tree to improve clinical outcomes. *Int J Radiat Oncol Biol Phys*. 2010; 76(2): 631-637.
[CrossRef] [PubMed Abstract]

[80] Campbell AM, Bailey IH, Burton MA. Analysis of the distribution of intra-arterial microspheres in human liver following hepatic yttrium-90 microsphere therapy. *Phys Med Biol.* 2000; 45(4): 1023-1033.
[CrossRef] [PubMed Abstract]

[81] Campbell AM, Bailey IH, Burton MA. Tumour dosimetry in human liver following hepatic yttrium-90 microsphere therapy. *Phys Med Biol*. 2001; 46(2): 487-498.
[CrossRef] [PubMed Abstract]

[82] Högberg J, Rizell M, Hultborn R, et al. Heterogeneity of microsphere distribution in resected liver and tumour tissue following selective intrahepatic radiotherapy. *EJNMMI Research*. 2014; 4: 48.
[Reference Source]

[83] Sarrut D, Bardies M, Boussion N, et al. A review of the use and potential of the GATE Monte Carlo simulation code for radiation therapy and dosimetry applications. *Med Phys*. 2014; 41(6): 064301.
[CrossRef] [PubMed Abstract]

[84] Parach AA, Rajabi H, Askari MA. Assessment of MIRD data for internal dosimetry using the GATE Monte Carlo code. *Radiat Environ Biophys*. 2011; 50(3): 441-450.
[CrossRef] [PubMed Abstract]

[85] Gulec SA, Sztejnberg ML, Siegel JA, Jevremovic T, Stabin M. Hepatic structural dosimetry in (90)Y microsphere treatment: a Monte Carlo modeling approach based on lobular microanatomy. *J Nucl Med*. 2010; 51(2): 301-310.
[Reference Source] [PubMed Abstract]

[86] Liu CS, Lin KH, Lee RC, et al. Model-based radiation dose correction for yttrium-90 microsphere treatment of liver tumors with central necrosis. *Int J Radiat Oncol Biol Phys*. 2011; 81(3): 660-668.
[CrossRef] [PubMed Abstract]

[87] Sanchez-Garcia M, Gardin I, Lebtahi R, Dieudonne A. A new approach for dose calculation in targeted radionuclide therapy (TRT) based on collapsed cone superposition: validation with ^{90}Y. *Phys Med Biol*. 2014; 59(17): 4769-4784.
[Reference Source] [PubMed Abstract]

[88] Petitguillaume A, Bernardini M, Hadid L, de Labriolle-Vaylet C, Franck D, Desbree A. Three-dimensional personalized Monte Carlo dosimetry in ^{90}Y resin microspheres therapy of hepatic metastases: nontumoral liver and lungs radiation protection considerations and treatment planning optimization. *J Nucl Med*. 2014; 55(3): 405-413.
[CrossRef] [PubMed Abstract]

[89] Prideaux AR, Song H, Hobbs RF, et al. Three-dimensional radiobiologic dosimetry: application of radiobiologic modeling to patient-specific 3-dimensional imaging-based internal dosimetry. *J Nucl Med*. 2007; 48(6): 1008-1016.
[CrossRef] [PubMed Abstract]

[90] Dieudonne A, Hobbs RF, Bolch WE, Sgouros G, Gardin I. Fine-resolution voxel S values for constructing absorbed dose distributions at variable voxel size. *J Nucl Med.* 2010; 51(10): 1600-1607.
[CrossRef] [PubMed Abstract]

[91] Dieudonne A, Hobbs RF, Lebtahi R, et al. Study of the impact of tissue density heterogeneities on 3-dimensional abdominal dosimetry: comparison between dose kernel convolution and direct Monte Carlo methods. *J Nucl Med*. 2013; 54(2): 236-243.
[CrossRef] [PubMed Abstract]

[92] Bolch WE, Bouchet LG, Robertson JS, et al. MIRD Pamphlet No. 17: The Dosimetry of Nonuniform Activity Distributions - Radionuclide S Values at the Voxel Level. *J Nucl Med*. 1999; 40(1): 11S-36S.
[Reference Source] [PubMed Abstract]

[93] Pacilio M, Lanconelli N, Lo Meo S, et al. Differences among Monte Carlo codes in the calculations of voxel S values for radionuclide targeted therapy and analysis of their impact on absorbed dose evaluations. *Med Phys*. 2009; 36(5): 1543-1552.
[CrossRef] [PubMed Abstract]

[94] Lanconelli N, Pacilio M, Lo Meo S, et al. A free database of radionuclide voxel S values for the dosimetry of nonuniform activity distributions. *Phys Med Biol*. 2012; 57(2): 517-533.
[CrossRef] [PubMed Abstract]

[95] Fernandez M, Hanscheid H, Mauxion T, et al. A fast method for rescaling voxel S values for arbitrary voxel sizes in targeted radionuclide therapy from a single Monte Carlo calculation. *Med Phys*. 2013; 40(8): 082502.
[CrossRef] [PubMed Abstract]

[96] Dieudonne A, Garin E, Laffont S, et al. Clinical feasibility of fast 3-dimensional dosimetry of the liver for treatment planning of hepatocellular carcinoma with ^{90}Y-microspheres. *J Nucl Med.* 2011; 52(12): 1930-1937.
[CrossRef] [PubMed Abstract]

[97] Gardin I, Bouchet LG, Assie K, et al. Voxeldose: A computer program for 3-D dose calculation in therapeutic nuclear medicine. *Cancer Biother Radiopharm.* 2003; 18(1): 109-115.
[CrossRef] [PubMed Abstract]

[98] Frisch KJ, Denis-Bacelar AM, Falzone N, Gear J, Flux G. qDose - a Software Application for 3D Dosimetry in Radionuclide Therapy. Annual Congress of the European Association of Nuclear Medicine. Gothenburg, Sweden; 2014. p. OP270.
[Reference Source]

[99] Kletting P, Schimmel S, Kestler HA, et al. Molecular radiotherapy: the NUKFIT software for calculating the time-integrated activity coefficient. *Med Phys*. 2013; 40(10): 102504.
[CrossRef] [PubMed Abstract]

[100] Gulec SA, Siegel JA. Posttherapy radiation safety considerations in radiomicrosphere treatment with ^{90}Y-microspheres. *J Nucl Med*. 2007; 48(12): 2080-2086.
[CrossRef] [PubMed Abstract]

[101] Pasciak AS, Bourgeois AC, Bradley YC. A Comparison of Techniques for (90)Y PET/CT Image-Based Dosimetry Following Radioembolization with Resin Microspheres. *Front Oncol.* 2014; 4: 121.
[Reference Source] [PubMed Abstract]

[102] Pasciak AS, Erwin WD. Effect of voxel size and computation method on Tc-99m MAA SPECT/CT-based dose estimation for Y-90 microsphere therapy. *IEEE Trans Med Imaging*. 2009; 28(11): 1754-1758.
[CrossRef] [PubMed Abstract]

[103] Bourgeois AC, Chang TT, Bradley YC, Acuff SN, Pasciak AS. Intraprocedural yttrium-90 positron emission tomography/CT for treatment optimization of yttrium-90 radioembolization. *J Vasc Interv Radiol.* 2014; 25(2): 271-275.
[CrossRef] [PubMed Abstract]

[104] Kao YH. Results confounded by a disregard for basic dose-response radiobiology. *J Nucl Med*. 2013; 54(9): 1682-1683.
[CrossRef] [PubMed Abstract]

[105] Lam MGEH, Smits MLJ. Value of ^{99m}Tc-Macroaggregated Albumin SPECT for Radioembolization Treatment Planning. *J Nucl Med.* 2013; 54(9): 1681-1682.
[CrossRef] [PubMed Abstract]

[106] Ulrich G, Dudeck O, Grosser O, Amthauer H. Reply: Value of ^{99m}Tc-macroaggregated albumin SPECT for radioembolization treatment planning. *J Nucl Med.* 2013; 54(9): 1682.
[CrossRef] [PubMed Abstract]

[107] Ulrich G, Dudeck O, Grosser O, Amthauer H. Reply: Results confounded by a disregard for basic dose-response radiobiology. *J Nucl Med*. 2013; 54(9): 1683-1684.
[CrossRef] [PubMed Abstract]

[108] Garin E, Lenoir L, Rolland Y, et al. Dosimetry based on ^{99m}Tc-macroaggregated albumin SPECT/CT accurately predicts tumor response and survival in hepatocellular carcinoma patients treated with ^{90}Y-loaded glass microspheres: preliminary results. *J Nucl Med*. 2012; 53(2): 255-263.
[CrossRef] [PubMed Abstract]

[109] Garin E, Lenoir L, Edeline J, et al. Boosted selective internal radiation therapy with ^{90}Y-loaded glass microspheres (B-SIRT) for hepatocellular carcinoma patients: a new personalized promising concept. *Eur J Nucl Med Mol Imaging*. 2013; 40(7): 1057-1068.
[CrossRef] [PubMed Abstract]

[110] Mazzaferro V, Sposito C, Bhoori S, et al. Yttrium-90 radioembolization for intermediate-advanced hepatocellular carcinoma: a phase 2 study. *Hepatology.* 2013; 57(5): 1826-1837.
[CrossRef] [PubMed Abstract]

[111] Lam MG, Goris ML, Iagaru AH, Mittra ES, Louie JD, Sze DY. Prognostic utility of ^{90}Y radioembolization dosimetry based on fusion ^{99m}Tc-macroaggregated albumin-99mTc-sulfur colloid SPECT. *J Nucl Med*. 2013; 54(12): 2055-2061.
[CrossRef] [PubMed Abstract]

[112] Flamen P, Vanderlinden B, Delatte P, et al. Multimodality imaging can predict the metabolic response of unresectable colorectal liver metastases to radioembolization therapy with Yttrium-90 labeled resin microspheres. *Phys Med Biol.* 2008; 53(22): 6591-6603.
[CrossRef] [PubMed Abstract]

[113] Lassmann M, Strigari L, Bardies M. Dosimetry is alive and well. *Cancer Biother Radiopharm*. 2010; 25(5): 593-595.
[CrossRef] [PubMed Abstract]

[114] Wessels BW, Konijnenberg MW, Dale RG, et al. MIRD Pamphlet No. 20: The Effect of Model Assumptions on Kidney Dosimetry and Response—Implications for Radionuclide Therapy. *J Nucl Med.* 2008; 49(11): 1884-1899.
[Reference Source] [PubMed Abstract]

[115] Di Dia A, Cremonesi M, Botta F, et al. Impact of 3D dosimetric and radiobiological estimates methods in radioembolisation of liver metastasis with ^{90}Y- microspheres. *Eur J Nucl Med Mol Imaging.* 2011; Suppl 2: OP022.
[Reference Source]

[116] Emami B, Lyman J, Brown A, et al. Tolerance of normal tissue to therapeutic irradiation. *Int J Radiat Oncol Biol Phys.* 1991; 21(1): 109-122.
[CrossRef] [PubMed Abstract]

[117] Bagni O, D'Arienzo M, Chiaramida P, et al. ^{90}Y-PET for the assessment of microsphere biodistribution after selective internal radiotherapy. *Nucl Med Commun.* 2012; 33(2): 198-204.
[Reference Source] [PubMed Abstract]

[118] Kao YH, Steinberg J, Tay YS, et al. Post-radioembolization yttrium-90 PET/CT - part 1: diagnostic reporting. *EJNMMI Res.* 2013; 3: 56.
[CrossRef] [PubMed Abstract]

[119] Gates VL, Esmail AA, Marshall K, Spies S, Salem R. Internal pair production of ^{90}Y permits hepatic localization of microspheres using routine PET: proof of concept. *J Nucl Med*. 2011; 52(1): 72-76.
[CrossRef] [PubMed Abstract]

[120] D'Arienzo M, Chiaramida P, Chiacchiararelli L, et al. ^{90}Y PET-based dosimetry after selective internal radiotherapy treatments. *Nucl Med Commun*. 2012; 33(6): 633-640.
[Reference Source] [PubMed Abstract]

[121] van Elmbt L, Vandenberghe S, Walrand S, Pauwels S, Jamar F. Comparison of yttrium-90 quantitative imaging by TOF and non-TOF PET in a phantom of liver selective internal radiotherapy. *Phys Med Biol.* 2011; 56(21): 6759-6777.
[Reference Source] [PubMed Abstract]

[122] Carlier T, Eugène T, Bodet-Milin C, et al. Assessment of acquisition protocols for routine imaging of Y-90 using PET/CT. *EJNMMI Res.* 2013; 3: 11.
[CrossRef] [PubMed Abstract]

[123] Tapp KN, Lea WB, Johnson MS, Tann M, Fletcher JW, Hutchins GD. The Impact of Image Reconstruction Bias on PET/CT ^{90}Y Dosimetry After Radioembolization. *J Nucl Med.* 2014; 55(9): 1452-1458.
[CrossRef] [PubMed Abstract]

[124] Lhommel R, van Elmbt L, Goffette P, et al. Feasibility of ^{90}Y TOF PET-based dosimetry in liver metastasis therapy using SIR-Spheres. *Eur J Nucl Med Mol Imaging*. 2010; 37(9): 1654-1662.
[CrossRef] [PubMed Abstract]

[125] Lea WB, Tapp KN, Tann M, Hutchins GD, Fletcher JQ, Johnson MS. Microsphere Localization and Dose Quantification Using Positron Emission Tomography/CT following Hepatic Intraarterial Radioembolization with Yttrium-90 in Patients with Advanced Hepatocellular Carcinoma. *J Vasc Interv Radiol*. 2014; 25(10): 1595-1603.
[CrossRef] [PubMed Abstract]

[126] Fourkal E, Veltchev I, Lin M, et al. 3D inpatient dose reconstruction from the PET-CT imaging of ^{90}Y microspheres for metastatic cancer to the liver: feasibility study. *Med Phys.* 2013; 40(8): 081702.
[CrossRef] [PubMed Abstract]

[127] Pasciak AS, Bourgeois AC, McKinney JM, et al. Radioembolization and the Dynamic Role of (90)Y PET/CT. *Front Oncol*. 2014; 4: 38.
[Reference Source] [PubMed Abstract]

[128] Avila-Rodriguez MA, Selwyn RG, Hampel JA, et al. Positron-emitting resin microspheres as surrogates of ^{90}Y SIR-Spheres: a radiolabeling and stability study. *Nucl Med Biol*. 2007; 34(5): 585-590.
[CrossRef] [PubMed Abstract]

[129] Avila-Rodriguez MA, Selwyn RG, Converse AK, Nickles RJ. ^{86}Y and ^{89}Zr as PET Imaging Surrogates for ^{90}Y: A Comparative Study. *AIP Conf Proc.* 2006; 854: 45.
[CrossRef]

[130] Selwyn RG, Avila-Rodriguez MA, Converse AK, et al. ^{18}F-labeled resin microspheres as surrogates for ^{90}Y resin microspheres used in the treatment of hepatic tumors: a radiolabeling and PET validation study. *Phys Med Biol.* 2007; 52(24): 7397-7408.
[CrossRef] [PubMed Abstract]

[131] Walrand S, Flux GD, Konijnenberg MW, et al. Dosimetry of yttrium-labelled radiopharmaceuticals for internal therapy: ^{86}Y or ^{90}Y imaging? *Eur J Nucl Med Mol Imaging*. 2011; 38 Suppl 1: S57-68.
[CrossRef] [PubMed Abstract]

[132] Amor-Coarasa A, Milera A, Carvajal D, Gulec S, Leichner J, McGoron AJ. (68)Ga-NOTA-CHSg and (99m)Tc-CHSg Labeled Microspheres for Lung Perfusion and Liver Radiomicrospheres Therapy Planning. *Int J Mol Imaging.* 2013; 2013: 279872.
[Reference Source] [PubMed Abstract]

[133] Zielhuis SW, Nijsen JF, de Roos R, et al. Production of GMP-grade radioactive holmium loaded poly(L-lactic acid) microspheres for clinical application. *Int J Pharm.* 2006; 311(1-2): 69-74.
[CrossRef] [PubMed Abstract]

[134] Smits ML, Nijsen JF, van den Bosch MA, et al. Holmium-166 radioembolization for the treatment of patients with liver metastases: design of the phase I HEPAR trial. *J Exp Clin Cancer Res*. 2010; 29: 70.
[CrossRef] [PubMed Abstract]

[135] Guimarães CC, Moralles M, Martinelli JR. Monte Carlo simulation of liver cancer treatment with ^{166}Ho-loaded glass microspheres. *Radiation Physics and Chemistry*. 2014; 95: 185-187.
[Reference Source]

[136] Vente MA, de Wit TC, van den Bosch MA, et al. Holmium-166 poly(L-lactic acid) microsphere radioembolisation of the liver: technical aspects studied in a large animal model. *Eur Radiol.* 2010; 20(4): 862-869.
[CrossRef] [PubMed Abstract]

[137] Smits MLJ, Nijsen JFW, van den Bosch MA, et al. Holmium-166 radioembolisation in patients with unresectable, chemorefractory liver metastases (HEPAR trial): a phase 1, dose-escalation study. *The Lancet Oncology*. 2012; 13(10): 1025-1034.
[CrossRef] [PubMed Abstract]

[138] Smits ML, Elschot M, van den Bosch MA, et al. In vivo dosimetry based on SPECT and MR imaging of ^{166}Ho-microspheres for treatment of liver malignancies. *J Nucl Med*. 2013; 54(12): 2093-2100.
[CrossRef] [PubMed Abstract]

[139] Ferreira MCM, Podder TK, Rasmussen KH, Jung JW. Praseodymium-142 microspheres for brachytherapy of nonresectable hepatic tumors. *Brachytherapy*. 2013; 12(6): 654-664.
[CrossRef] [PubMed Abstract]

[140] Rose SC, Kikolski SG, Chomas JE. Downstream hepatic arterial blood pressure changes caused by deployment of the surefire antireflux expandable tip. *Cardiovasc Intervent Radiol*. 2013; 36(5): 1262-1269.
[CrossRef] [PubMed Abstract]

[141] van den Hoven AF, Prince JF, Samim M, et al. Posttreatment PET-CT-confirmed intrahepatic radioembolization performed without coil embolization, by using the antireflux Surefire Infusion System. *Cardiovasc Intervent Radiol*. 2014; 37(2): 523-528.
[Reference Source] [PubMed Abstract]

[142] Lewandowski RJ, Minocha J, Memon K, et al. Sustained safety and efficacy of extended-shelf-life (90)Y glass microspheres: long-term follow-up in a 134-patient cohort. *Eur J Nucl Med Mol Imaging*. 2014; 41(3): 486-493.
[Reference Source] [PubMed Abstract]

[143] Kao YH. A Clinical Dosimetric Perspective Uncovers New Evidence and Offers New Insight in Favor of ^{99m}Tc-Macroaggregated Albumin for Predictive Dosimetry in ^{90}Y Resin Microsphere Radioembolization. *J Nucl Med*. 2013; 54(12): 2191-2192.
[CrossRef] [PubMed Abstract]

[144] Lassmann M, Chiesa C, Flux G, Bardies M, Committee ED. EANM Dosimetry Committee guidance document: good practice of clinical dosimetry reporting. *Eur J Nucl Med Mol Imaging*. 2011; 38(1): 192-200.
[CrossRef] [PubMed Abstract]

[145] Ricke J, Grosser O, Amthauer H. ^{90}Y-radioembolization of lung metastases via the bronchial artery: a report of 2 cases. *Cardiovasc Intervent Radiol*. 2013; 36(6): 1664-1669.
[CrossRef] [PubMed Abstract]

[146] Joulaeizadeh L, Bobin C, Capogni M, et al. Traceable dosimetry for Molecular Radiotherapy. European Association of Nuclear Medicine Annual Meeting. Gothenburg, Sweden; 2014.
[Reference Source]

[147] Villoing D, McParland B, Suhard J, Ferrer L, Bardiès M. Dosimetric calculation with Monte Carlo simulation of a PET radiotracer: Comparison between the standard and the personalized approach. Proceedings of the European Association of Nuclear Medicine Congress. Milan, Italy; 2012.
[Reference Source]

[148] Gates VL, Marshall KG, Salzig K, Williams M, Lewandowski RJ, Salem R. Outpatient single-session yttrium-90 glass microsphere radioembolization. *J Vasc Interv Radiol*. 2014; 25(2): 266-270.
[CrossRef] [PubMed Abstract]

Citation: O' Doherty J. A review of 3D image-based dosimetry, technical considerations and emerging perspectives in ^{90}Y microsphere therapy. *Journal of Diagnostic Imaging in Therapy*. 2015; 2(2): 1-34.

DOI: http://dx.doi.org/10.17229/jdit.2015-0428-016

Received: 08 April 2015 | **Revised:** 27 April 2015 | **Accepted:** 28 April 2015

Published Online 28 April 2015 http://www.openmedscience.com